REVIEW SUMMARY

MAGNETISM

Two-dimensional magnetic crystals and emergent heterostructure devices

Cheng Gong and Xiang Zhang*

BACKGROUND: The electron can be considered as a tiny magnet, with two opposite poles defining its magnetic field associated with the spin and orbital motion. When such minuscule magnets are collectively aligned as a result of the inherent coupling, ferromagnetism emerges. However, ferromagnetism had long been believed to hardly survive in two-dimensional (2D) systems because of the enhanced thermal fluctuations revealed by the Mermin-Wagner theorem. The recent discovery of 2D magnetic crystals showed that magnetic anisotropy could stabilize the long-range magnetic order by opening up an excitation gap to resist the thermal agitation. Two-dimensional magnetic crystals constitute ideal platforms to experimentally access the fundamental physics of magnetism in reduced dimensions. In contrast to the traditional magnetic thin films, 2D materials largely decouple from the substrates, allow electrical control, are mechanically flexible, and are open to chemical functionalization. These attributes make 2D magnets accessible, engineerable, and integrable into emergent heterostructures for previously unachieved properties and applications such as atomically thin magneto-optical and magnetoelectric devices for ultracompact spintronics, on-chip optical communications, and quantum computing.

ADVANCES: Magnetism has been explored in 2D materials for more than a decade. Magnetic moments have been created through defect engineering based on vacancies, adatoms, boundaries, and edges; band structure engineering, assisted by density functional theory calculations, has raised possibilities of 2D magnetism in, for instance, gated bilayer graphene and doped GaSe; the proximity effect has been applied to imprint spin polarization in 2D materials from magnetic substrates. However, these prior efforts centered on extrinsically induced magnetic response.

In early 2017, the first observations of long-range magnetic order in pristine 2D crystals were reported in $Cr_2Ge_2Te_6$ and CrI_3. Both are magnetic insulators, yet with distinct magnetic properties. In contrast, 2D Fe_3GeTe_2 was recently proven to be a magnetic conductor. Itinerant magnets and magnetic insulators possess diverse application perspectives. Molecular beam epitaxial growth of 2D magnets has been reported for Fe_3GeTe_2, VSe_2, $MnSe_x$, and $Cr_2Ge_2Te_6$. The typical Curie temperatures of 2D magnets are much lower than those of their 3D counterparts. However, this does not fundamentally exclude the possibility of high-temperature 2D magnets. Efforts toward this goal have shown promise.

When van der Waals (vdW) magnets contact nonmagnetic materials, time reversal asymmetry could be introduced in the original nonmagnets, likely leading to, for example, valley polarization in transition metal dichalcogenides or quantum anomalous Hall states in topological insulators. However, it should be noted that 2D magnets' properties are susceptible to the contacting materials. Stacking vdW magnets with dissimilar materials could enrich the landscape of emergent phenomena by causing, for example, heterostructure multiferroicity, unconventional superconductivity, and the quantum anomalous Hall effect.

Two-dimensional spintronic and magnonic devices have begun to emerge. Spin-orbit torque has been generated while spin-polarized current is injected from 2D materials (e.g., WTe_2) into magnetic substrates; conversely, a spin wave has been pumped from magnetic substrates into 2D materials for spin-charge conversion. Magnetic tunnel junctions with 2D magnets (e.g., CrI_3) as tunneling barriers exhibit giant tunneling magnetoresistance at low temperatures. New concepts of spin field-effect transistors based on 2D magnets have been reported as well.

ON OUR WEBSITE

Read the full article at http://dx.doi.org/10.1126/science.aav4450

OUTLOOK: Most currently available 2D magnets rely on mechanical exfoliation and only work at low temperatures. The wafer-scale synthesis of 2D magnets that operate above room temperature is a prerequisite for the development of practical applications. In the longer run, the monolithic integration of such 2D magnets with other functional materials is crucial for practical scalability. Spintronic devices require efficient electrical modulation of 2D magnets, long-distance transport of spins or spin waves, and efficient tunneling and injection of spins at various junctions. The practical development of low-power spintronic devices needs to be compatible with the existing complementary metal-oxide semiconductor technology (e.g., impedance match and affordable power supply). Furthermore, the exotic spin textures, quantum phases, and quasiparticles in 2D magnetic crystals and hetero-interfaces could lead to new ways of computation and communication. We envision that successive breakthroughs in 2D magnets could usher in a new era of information technologies with exciting applications in computing, sensing, and data storage. ■

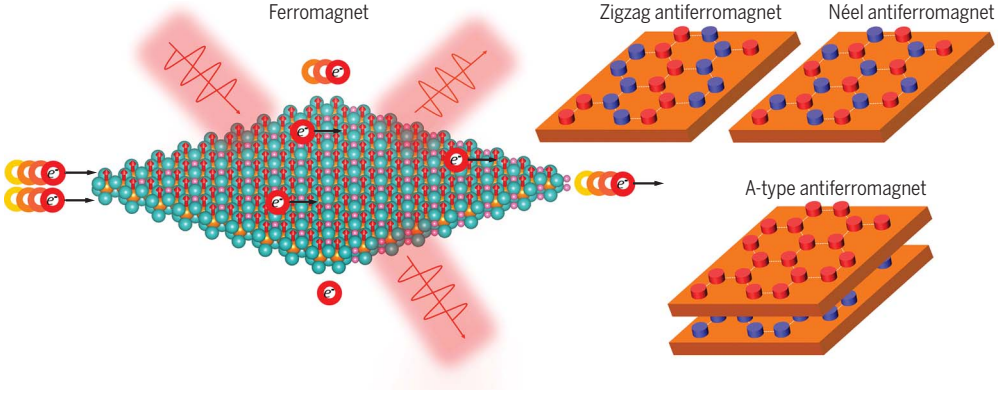

Two-dimensional magnetic crystals: The atomically thin crystalline hosts of magneto-optic and magnetoelectric effects. 2D magnetic crystals, including 2D ferromagnets (left) and 2D antiferromagnets with diverse intra- and interplane magnetic configurations (right), can exhibit a plethora of magneto-optic and magnetoelectric effects. The red and blue protrusions in the atomic Lego depict the opposite local spins in magnetic layers.

The list of author affiliations is available in the full article online.
*Corresponding author. Email: xiang@berkeley.eu
Cite this article as C. Gong and X. Zhang, *Science* **363**, eaav4450 (2019). DOI: 10.1126/science.aav4450

REVIEW

MAGNETISM

Two-dimensional magnetic crystals and emergent heterostructure devices

Cheng Gong[1] and Xiang Zhang[1,2]*

Magnetism, originating from the moving charges and spin of elementary particles, has revolutionized important technologies such as data storage and biomedical imaging, and continues to bring forth new phenomena in emergent materials and reduced dimensions. The recently discovered two-dimensional (2D) magnetic van der Waals crystals provide ideal platforms for understanding 2D magnetism, the control of which has been fueling opportunities for atomically thin, flexible magneto-optic and magnetoelectric devices (such as magnetoresistive memories and spin field-effect transistors). The seamless integration of 2D magnets with dissimilar electronic and photonic materials opens up exciting possibilities for unprecedented properties and functionalities. We review the progress in this area and identify the possible directions for device applications, which may lead to advances in spintronics, sensors, and computing.

For centuries, humans had been puzzled about the magic attraction of lodestones to iron, and perhaps even more about the fascinating ability of birds, fish, and insects to navigate between destinations of thousands of miles apart. In early times before the development of electromagnetism and quantum mechanics, it was hard to imagine that these intriguing phenomena may share a common magnetic origin. Magnetism is fundamentally rooted in the moving charges and spin of elementary particles; hence, it is as ubiquitous as the electron itself. It has found broad applications in living organisms as well as in energy harvesting, data storage, and medical diagnosis. When the infinitesimal "electron magnets" are spontaneously aligned, the magnetic order constitutes a fundamental phase of matter, giving rise to a host of functional devices including electric generators and motors, magnetoresistive memories, and optical isolators. The ability to knit such magnetic order in atomically thin flatlands would foster vast opportunities for integrated, flexible, and biocompatible devices; however, such two-dimensional (2D) magnets are not easily attainable because of a fundamental hindrance.

Understanding the fundamental difference between 2D and 3D magnetism is instructive. The driving force underlying the ordering of electrons' spin magnetic moments in an (anti-)ferromagnet is the "exchange interaction," which was initially dubbed as a "molecular field" by Pierre Weiss in 1907 (*1*) and was understood to be of quantum mechanical origin in 1926 (*2*, *3*) (Fig. 1A). The effect is a coulombic interaction under the Pauli exclusion principle relating to the electrons' antisymmetric wave function. The exchange interaction has been used to estimate the Curie temperatures of 3D ferromagnets, based on the argument that the short-range exchange interaction needs to be overcome by thermal energy to randomize the magnetic moments. Nonetheless, the mean-field picture suitable for 3D systems does not work for the length scale of 2D systems, in which the dimensionality effect comes into play (*4*). Magnon (i.e., quanta of spin wave) dispersion in 2D systems is reduced with respect to that in the 3D counterparts, corresponding to an abrupt onset of magnon density of states (DOS) in 2D systems and thus an ease of thermal agitations (*5*, *6*). For 2D systems without magnetic anisotropy (Fig. 1B), the spin wave excitation gap diminishes (Fig. 1C). Together with the diverging Bose-Einstein statistics of magnons at zero energy, any nonzero temperatures cause massive magnon excitations and the spin ordering to collapse, as predicted by Mermin and Wagner (*4*). However, for 2D systems with a uniaxial magnetic anisotropy, a magnon excitation gap opens up and resists the thermal agitations (Fig. 1, D and E), which then lifts the Mermin-Wagner restriction and results in finite Curie temperatures. Meanwhile, the exchange interaction together with the dimensionality dictates the magnon band width and profiles (*6*). Therefore, the synergy of these factors, as well as the inter(quasi-)particle scattering, which potentially renormalizes the magnon spectrum, determines the upper bound temperature (i.e., Curie temperature) below which a 2D ferromagnet can be found.

The past a few decades have witnessed the role of epitaxial thin films and superlattices as testing grounds for the experimental exploration of 2D magnetic properties and spin entity (i.e., spin-polarized electrons or spin waves) propagations. Seminal phenomena such as giant magnetoresistance (*7*, *8*), the dimensionality effect (*9*–*11*), and oscillating exchange coupling (*12*) were discovered. But it has been a long-standing challenge to access the intrinsic magnetic properties of ultrathin films as a pure quantum confinement effect of their 3D counterparts; these traditional thin films suffer from various perturbations such as interfacial hybridization, electronic redistribution, reduced coordination with band narrowing, atomic interdiffusion, strain, crystalline reconstruction, finite-size islands (typically tens of nanometers), and irregular shapes (*13*, *14*). Therefore, the properties of such ultrathin films are difficult to precisely control and replicate.

In stark contrast, the recently discovered 2D magnetic atomic crystals (*6*, *15*) provide unique opportunities for both fundamental physics and technological advances. Such magnetically ordered atomic crystals enable unprecedented experimental access to the ground states, fundamental excitations, and magnon dynamics of single-crystalline 2D magnets. Because such 2D magnetic crystals are susceptible to a long list of external stimuli including mechanical deformation, electrostatic doping, light incidence, chemical decoration, and dielectric environment, there is enormous room to engineer 2D magnets for desired properties; the sensitive responses of 2D magnets allow the development of miniaturized, lightweight, flexible, and biocompatible devices based on magnetoresistive, magnetoelectric, magnetostrictive, magneto-optical, and magnetobiological effects. Furthermore, the past decade has witnessed the increasingly skillful handling of individual 2D layers, which could facilitate the unprecedented fabrication of multilayer "designer magnets"; a notable outcome could be the giant cross-layer tunneling magnetoresistance by designing the interlayer magnetic coupling. In heterostructures with electronic and photonic materials, the seamless integration and intricate interplay of distinct physical properties could give rise to emergent interfacial phenomena such as heterostructure multiferroicity, unconventional superconductivity, and the quantum anomalous Hall effect. It is reasonable to envision that a vast range of previously unachieved properties will be discovered in 2D magnetic crystals, derivatives, and heterointerfaces, which could be transformed into a host of applications such as low-power spintronics, on-chip optical communications, and quantum computing.

Induced magnetic response in nonmagnetic 2D materials

Since the advent of graphene, attempts to create ferromagnetism in nonmagnetic 2D materials have continued apace. One of the mainstream strategies is through introducing vacancies or adding adatoms such as hydrogen and fluorine (*16*–*22*) (Fig. 2, A and B). Such defect engineering produces local magnetic moments from unpaired electrons, which, for example, could be further correlated through conduction electrons in graphene (itinerant π-magnetism). However, attempts to order these moments in a "long-range"

[1]Nanoscale Science and Engineering Center, University of California, Berkeley, CA 94720, USA. [2]Faculties of Science and Engineering, University of Hong Kong, Hong Kong, P.R. China.
*Corresponding author. Email: xiang@berkeley.edu

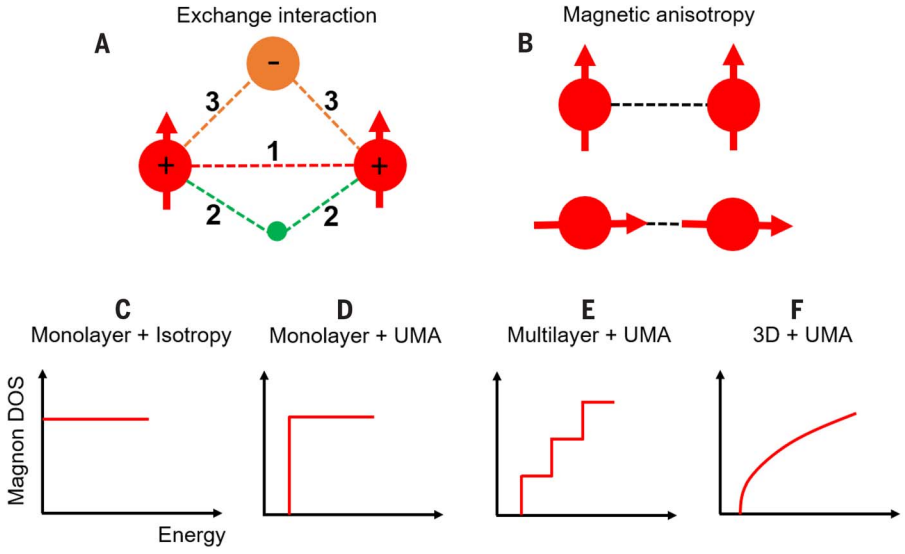

Fig. 1. Fundamental physical parameters and spin wave excitations in ferromagnets of different dimensionalities. (**A** and **B**) In a collinear magnet, exchange interaction and magnetic anisotropy are fundamental parameters. Exchange interaction arises from electrons' antisymmetric wave function and is governed by coulombic interaction under the Pauli exclusion principle. Exchange interaction between spins can be directly established (red dashed line 1) or indirectly mediated by conduction electrons (green ball with dashed lines labeled 2) or intermediate anions (orange ball with dashed lines labeled 3) such as O^{2-}. While spins are aligned, there is usually a preferred orientation, which means magnetic anisotropy. Magnetic anisotropy has a variety of sources such as magnetocrystalline anisotropy, shape anisotropy, and stress anisotropy. (**C** to **F**) In a 2D isotropic Heisenberg ferromagnet, there will be massive excitations of magnons at nonzero temperatures because of the absence of a spin wave excitation gap, the abrupt onset of magnon density of states (DOS), and the diverging Bose-Einstein statistics at zero energy; the result is collapse of long-range magnetic order. The presence of uniaxial magnetic anisotropy (UMA) opens up the spin wave excitation gap to resist the thermal agitations of magnons, leading to the finite Curie temperature. As the system evolves from 2D to 3D, the magnon DOS spectrum changes from a step function to a gradually increasing function with zero DOS at the threshold of excitation. Therefore, in 3D systems, UMA (related to the spin wave excitation gap) is not a prerequisite for the presence of finite-temperature long-range magnetic order.

pattern posed overwhelming challenges in material preparation. One report (*23*) disagreed with the feasibility of these approaches to realizing long-range ferromagnetic order, because the authors only observed the paramagnetic response in graphene with fluorine adatoms or vacancies at liquid helium temperatures, and observed a maximum response of about 1 magnetic moment per 1000 atoms in all tested samples. Despite a number of prior reports on the observation of ferromagnetism in originally nonmagnetic 2D materials, no consensus has been reached (*24*, *25*). The primary debates center on the source of the detected magnetic signals: A chunk of material in a superconducting quantum interference device (SQUID) measurement chamber is typically hundreds of micrometers thick, approximately six orders of magnitude thicker than an atomic sheet. Hence, true signals from the 2D sheet may be overshadowed by ferromagnetic impurities in substrates, even if the impurity concentrations are as low as 10 ppm.

Flat band ferromagnetism has been proposed to be realized via extended defects such as zigzag edges of graphene nanoribbons or grain boundaries of 2D materials (*26*–*28*). Such defects cause less-dispersed electronic bands that satisfy the huge density of states in a narrow energy scope, leading to the Stoner instability toward a ferromagnetic phase. However, these chemically reactive defects are vulnerable to passivation by foreign species; also, long-range 1D ferromagnetic order cannot exist in theory (*26*). Although the strict "long-range" (i.e., infinitely long) ferromagnetic order is not allowed in 1D systems, it is possible to make magnetically ordered chains with finite length and width, so that the finite-size ferromagnets (*29*–*31*) behave as spin blocks of superparamagnets with reasonably long spin flipping time, which can provide a practical path toward nanoscale spintronic devices (*26*, *32*, *33*).

Band structure engineering may represent a vital route to create 2D ferromagnetism from originally nonmagnetic 2D materials, without the assistance of structural imperfections. For instance, such band ferromagnetism was predicted to exist in electrically biased bilayer graphene (*34*, *35*) (Fig. 2F) and doped GaSe (*36*, *37*). In bilayer graphene biased by electric fields perpendicular to the basal plane, the different electrostatic potentials experienced by the two layers induce a gap opening and a Mexican-hat dispersion at low energy. Such Mexican-hat bands are often concomitant with the itinerant ferromagnetism. Nonetheless, the anticipated ferromagnetic phase has not been experimentally observed thus far, likely because of the limited total magnetic moments or low Curie temperatures. The predicted magnetism in doped GaSe is based on the similar strategy of Mexican-hat band dispersion. However, ab initio calculations show the necessity of hole-doped GaSe up to 10^{13} to 10^{14} carriers/cm^2 to reach the van Hove singularity. Given the large quasiparticle band gap, 3.7 eV (*36*), it would be challenging to realize this high level of hole doping by conventional electrostatic schemes. Similar spontaneous valley polarization was observed in 2D electronic systems, such as the inversion layer in silicon in the 1970s (*38*). More recently, giant paramagnetism in monolayer MoS_2 was reported (*39*), with an unconfirmed yet possible spontaneous ferromagnetism proposed.

The magnetic proximity effect is a scheme to make nonmagnetic 2D materials magnetic by borrowing properties from adjacent magnetic materials. A graphene sheet, which was transferred on yttrium ion garnet (YIG) (*40*) (Fig. 2D) or upon which EuS was deposited (*41*) (Fig. 2E), exhibits an anomalous Hall effect. The sole evidence from an anomalous Hall signal does not suffice to conclude that a ferromagnetic phase in 2D materials exists, because other effects such as spin-dependent interfacial scattering or ferromagnetic impurities may result in similar observations (*42*). However, the quantification of the 14-T interfacial exchange field (*41*) and the observation of the quantum Hall effect at a much lower external magnetic field shed light on the presence of interfacial exchange fields. More direct evidence of the interfacial exchange field was subsequently obtained on the basis of spin current transport in lateral graphene spin valves on YIG (*43*, *44*). Interestingly, a spin dephasing mechanism due to the temporal and spatial fluctuation of interfacial exchange fields was revealed (*44*), which highlights from a new angle the critical role of interfacial quality in the spintronic transport properties of proximity systems.

Magnetism in pristine 2D materials

The first two reported 2D magnetic atomic crystals are chromium compounds: $Cr_2Ge_2Te_6$ (*6*) (Fig. 3, A to C) and CrI_3 (*15*) (Fig. 3, D and E). $Cr_2Ge_2Te_6$ is a 2D Heisenberg ferromagnet with small magnetic anisotropy (i.e., collectively aligned spin moments can be oriented toward all directions with small energy difference), whereas CrI_3 is probably a 2D Ising A-type antiferromagnet (i.e., spin moments oriented normal to the basal plane, intralayer ferromagnetism, and interlayer antiferromagnetism).

The slight distortion of the Cr-Te_6 octahedral cage, together with spin-orbit coupling on Cr ions, leads to a small out-of-plane magnetocrystalline anisotropy in $Cr_2Ge_2Te_6$. The nearly isotropic Heisenberg 2D ferromagnet mimics the ideal Mermin-Wagner condition, on the basis of which the external magnetic field has an

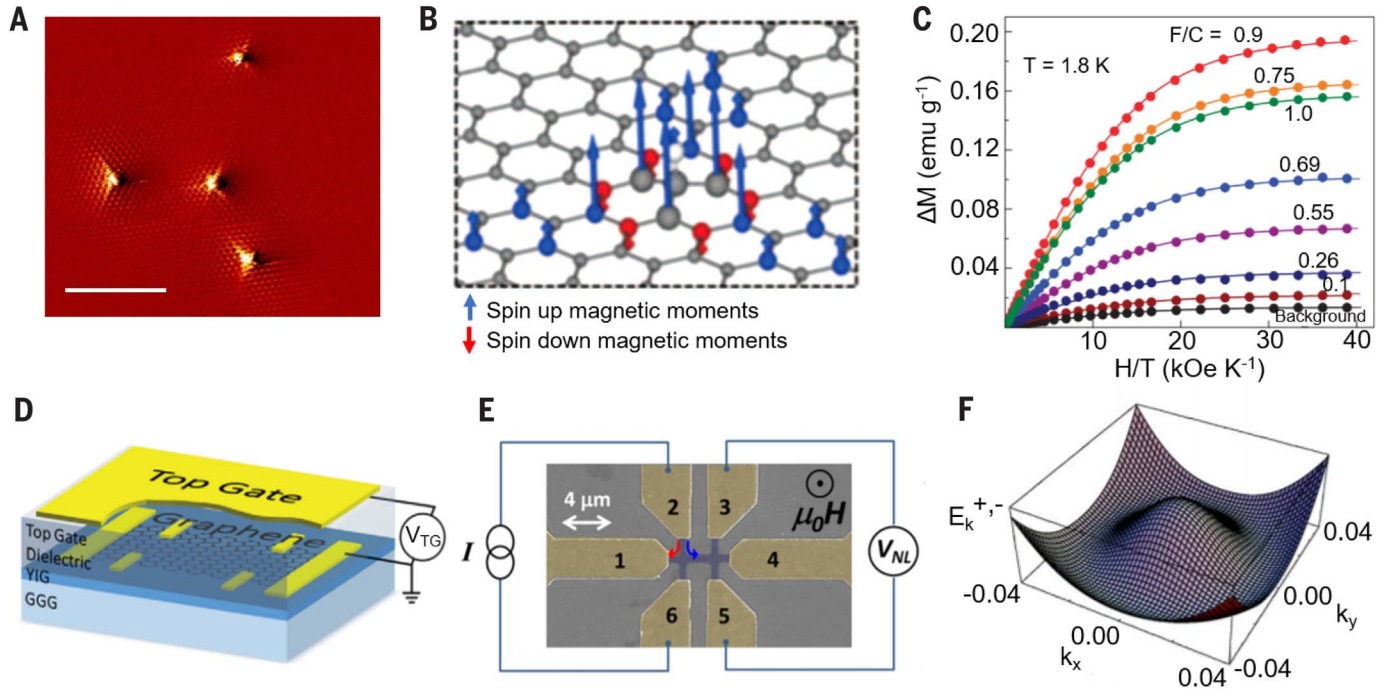

Fig. 2. Schemes to induce magnetism in nonmagnetic 2D materials. Point defects such as vacancies and adatoms in 2D materials are accompanied by defect states and local magnetic moments. (**A**) STM topography of graphene with carbon vacancies induced by Ar^+ ion irradiation (*17*). Scale bar, 5 nm. (**B**) Schematic of local magnetic moments in graphene decorated by an individual hydrogen adatom (small white ball at center) (*18*). The same spin-polarized state extends a few nanometers in carbon sites of the same sublattice, but the opposite spin-polarized state occupies the other carbon sublattice. (**C**) Magnetization versus magnetic field parallel to the fluorinated graphene planes (*23*). Dots are experimental data; solid lines are fitting curves based on Brillouin function. No trace of ferromagnetism was found in both fluorinated graphene and defective graphene with vacancies at liquid helium temperatures. (**D**) Schematic of a graphene field-effect transistor fabricated on YIG, a magnetic insulator (*40*). (**E**) Schematic of a graphene field-effect transistor covered by a deposited thin film of EuS, a magnetic insulator (*41*). Nonmagnetic 2D materials can be made magnetic by physically contacting magnetic materials through proximity effect. (**F**) Calculated Mexican-hat band dispersion in electrically biased Bernal stacked bilayer graphene (*34*). The diverging electronic DOS at the edge of the Mexican hat potentially results in ferromagnetic Stoner instability.

unprecedented effect on the observed transition temperatures of 2D $Cr_2Ge_2Te_6$. Despite possessing van der Waals (vdW) spacing, interlayer magnetic coupling is appreciable, as evidenced by the strong dimensionality effect in transition temperatures of $Cr_2Ge_2Te_6$ of different thickness. An isostructural compound, $Cr_2Si_2Te_6$ (*45*), has a larger easy-axis magnetic anisotropy and a lower bulk ferromagnetic phase transition temperature T_C at 33 K. The Curie temperature of the hypothetical isostructure $Cr_2Sn_2Te_6$ is theoretically predicted to be higher (*46*), but the successful synthesis of this crystal has not yet been reported.

The sizable magnetic anisotropy in CrI_3 was suggested to arise from the exchange anisotropy due to the spin-orbit interaction of iodine species that mediate the superexchange between Cr ions (*47*). Graphite-encapsulated few-layer CrI_3 shows interesting layer-contrasting magnetic properties and was suggested to be an A-type antiferromagnet. Further investigations are needed to identify the origin of the exotic properties of 2D CrI_3 that are contrary to those of its bulk counterpart [bulk CrI_3 is a ferromagnet (*48*)], although the altered interlayer registry in few-layer CrI_3 was invoked as a tentative explanation (*49*–*52*). Possible extrinsic causes relate to graphite capping, partial degradation (CrI_3 is extremely unstable to the moisture and light) (*53*), and unintentional doping and strain (especially for cases where CrI_3 samples were exfoliated on polymer and later transferred). The isostructural magnet $CrBr_3$ in bulk is an easy-axis ferromagnet with T_C = 33 K, and $CrCl_3$ in bulk is an easy-plane A-type antiferromagnet. Magnetic anisotropies and phase transition temperatures of bulk $CrCl_{(3-x)}Br_x$ alloys are tunable by changing stoichiometries (*54*).

Fe_3GeTe_2 is a metallic ferromagnet (*55*–*60*) (Fig. 3, F and G). In each layer, three of the quintuple sublayers are iron; the top and bottom sublayers are equivalent and the central one differs. The crystallographic environments of the iron atoms are asymmetric along and normal to the basal plane, leading to the sizable magnetocrystalline anisotropy. The tunable Curie temperatures and coercivities can be realized by varying the iron concentrations. Interestingly, in this 3*d* electronic system, the coexistence of itinerant ferromagnetism and Kondo lattice was evidenced (*61*), suggesting the presence of heavy fermions and periodically seated local moments. This constitutes an intriguing 2D material platform, in which itinerant electrons and local magnetic moments coexist and interplay, possibly leading to a plethora of emergent phases and phenomena.

Furthermore, for bulk Fe_3GeTe_2, evidence from magnetization characterization, electrical transport (*62*–*64*), scanning tunneling microscopy (STM) (*65*), and magnetic force microscopy (*63*) points to a different magnetic configuration emerging at even lower temperatures (~50 K lower than the Curie temperature of 220 to 230 K). The stripe domain phase in bulk Fe_3GeTe_2 observed by photoemission electron microscopy (*66*) indicates the quasi-2D magnetic behaviors, and the thickness-dependent magnetic hysteresis (*63*, *64*) reveals valuable hints that long-range dipolar interaction may play an important role when layers are stacked up to tens of nanometers.

In contrast to ferromagnets, antiferromagnets find limited applications—for example, to stabilize the "fixed layer" in spin valves and magnetic tunnel junctions. Despite the notorious difficulty in using antiferromagnets due to their net vanishing magnetization, antiferromagnets hold promise for high-speed, low-power spintronics because they have magnetic resonance frequencies in the terahertz regime, null stray field for vanishing cross-talk between adjacent bits, and robustness against the external magnetic field perturbation (*67*, *68*). Furthermore, antiferromagnets are much more abundant than ferromagnets.

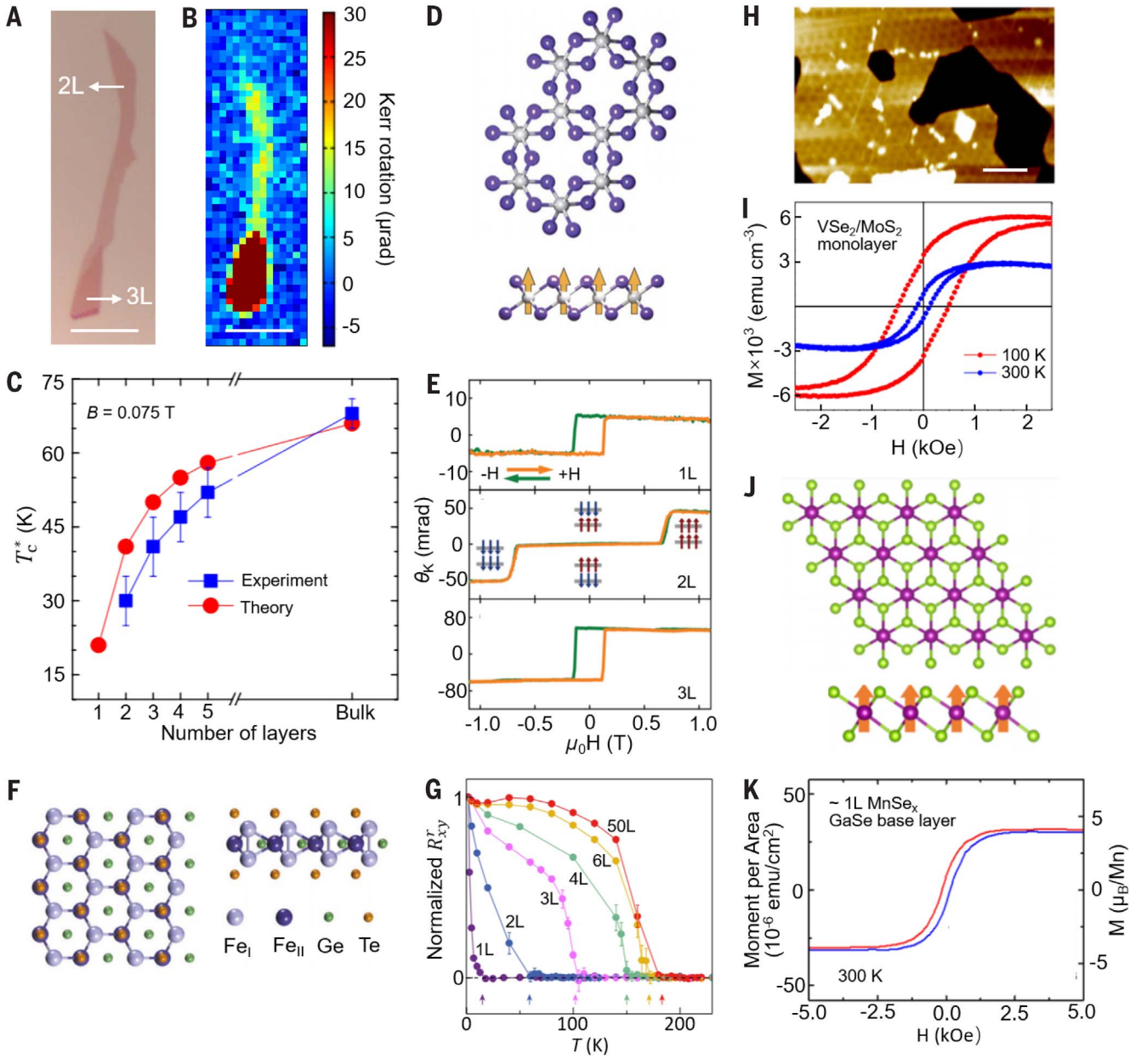

Fig. 3. Representative 2D magnetic crystals. (**A** to **C**) Optical image, Kerr image, and dimensionality effect of few-layer $Cr_2Ge_2Te_6$ exfoliated on SiO_2/Si (*6*). Scale bars, 10 μm. (**D** and **E**) Atomic structure of CrI_3 and thickness-dependent Kerr signal hysteresis loop of graphite-sandwiched 2D CrI_3 (*15*). In (D), orange arrows represent the ferromagnetically coupled spin magnetic moments. In (E), red and blue vertical arrows represent spin-up and spin-down magnetic moments, respectively. (**F** and **G**) Atomic structure of Fe_3GeTe_2 and thickness-dependent normalized remanent anomalous Hall resistance of 2D Fe_3GeTe_2 on Al_2O_3 thin film, which was prepared by thermally evaporating Al in oxygen pressure of 10^{-4} mbar on Fe_3GeTe_2 bulk crystal, followed by multiple steps of transfer and exfoliation (*62*). (**H** and **I**) STM image of sub-monolayer VSe_2 grown on HOPG by MBE and magnetic hysteresis of mostly monolayer VSe_2 grown on MoS_2 by MBE (*75*). Scale bar, 20 nm. (**J** and **K**) Atomic structure of vdW $MnSe_2$ and out-of-plane magnetic hysteresis of $MnSe_x$, one monolayer on average, grown on GaSe by MBE (*76*). In (J), orange arrows represent the ferromagnetically coupled spin magnetic moments. In (K), red and blue curves represent the half of the hysteresis loop while magnetic field is swept from positive to negative and from negative to positive, respectively.

Antiferromagnetic vdW materials are diverse in magnetic configurations such as the Ising antiferromagnets $FePS_3$ and $FePSe_3$ (*69*–*72*), the Heisenberg antiferromagnets $MnPS_3$ and $MnPSe_3$ (*72*, *73*), and the XY-type antiferromagnet $NiPS_3$ (*73*). Raman spectroscopy could provide nondestructive techniques to indirectly probe the magnetic phase transitions for some antiferromagnets. For example, $FePS_3$ has a Raman feature peak whose intensity has a sharp upturn when samples are cooled under Néel temperature (*74*). Methods that can effectively characterize antiferromagnetic order and magnetic excitations in atomically thin micrometer-size antiferromagnetic samples would be useful. Reading information from 2D antiferromagnets would pave the way to taking full advantage of the vdW antiferromagnets for ultrafast low-power spintronics.

An important consideration for the practical use of 2D magnets is the magnetic phase transition temperature. Substantial work has been devoted to enhancing the Curie temperatures of 2D ferromagnets beyond room temperature, with

a few claims of success thus far. For this ambitious goal, there appears to be no fundamental prohibition as long as the ferromagnetic exchange interaction and uniaxial magnetic anisotropy are strong enough. Yet the practical realization is not that easy. Room-temperature ferromagnetism was reported in single-layer 1T-VSe_2 synthesized on both highly oriented pyrolytic graphite (HOPG) and MoS_2 by molecular beam epitaxy (MBE) (*75*) (Fig. 3, H and I). Two puzzling points remain for this work: the unusually high magnetic moments (8000 emu/cm^3) in single-layer VSe_2 on MoS_2, and the observed easy-plane anisotropy, which can hardly sustain the long-range ferromagnetic order at room temperature unless a strong uniaxial anisotropy is present within the basal plane. In another contemporary study, the vdW phase of single-layer $MnSe_x$ was synthesized by MBE (*76*) (Fig. 3, J and K). Interestingly, such a vdW phase for $MnSe_x$ only exists in ultrathin layers, but the bulk counterparts prefer rock-salt NaCl or the hexagonal NiAs phase, both of which are antiferromagnetic (*77*). This observation highlights that 2D materials could exhibit novel structural forms that are not present in bulk, and thus possess unusual physical properties. For MBE samples, the possibly complicated interfaces formed during sample synthesis (e.g., by atomic diffusion, reaction, and alloying) should be carefully examined as the probable causes of the observed magnetic signals. A recent work (*78*) pointed out the magnetic element in a hot cell as a source of magnetic impurities in MBE synthesis.

In theory, there is not a fundamental restriction to 2D long-range magnetic order at high temperatures, although enhanced thermal fluctuations are always a hindrance. The rule of thumb in designing high-temperature 2D ferromagnets is to strengthen the exchange interaction and uniaxial magnetic anisotropy. Given the extensive prior experience in creating magnetic moments and enhancing spin-orbit coupling in graphene and other nonmagnetic 2D materials, it is safe to envision that thermally robust 2D ferromagnets will be discovered in ever more engineered 2D material systems.

Magnetism as a result of many-body interaction suggests electron correlation effects. Spin-charge coupling has been evidenced in $NiPS_3$ (*79*), an easy-plane antiferromagnet, showing the presence of electron correlations. Antiferromagnetism and strong electron correlations are reminiscent of unconventional superconductors. Interestingly, a recent experiment showed that $FePSe_3$, a vdW antiferromagnet, indeed evolves to be superconducting under hydrostatic pressure above 9 GPa (*80*). For ferromagnetic $Cr_2Ge_2Te_6$, the sharp upturn of electrical resistivity when temperature is lowered to a certain point above T_C suggests the spin-charge coupling (*81*). Strong electron correlations are implied by the enhanced electronic specific heat of Fe_3GeTe_2 with respect to that of nonmagnetic isostructural Ni_3GeTe_2, and are also supported by the comparison between experimental and calculated Sommerfeld coefficients in Fe_3GeTe_2 (*57*). Therefore, on the basis of all of this evidence, electron correlations appear generally present in 2D magnetic crystals. Such electron correlations enrich the complex phase diagrams, allow the electrical tuning and compositional engineering to switch between multiple phases, and make heterostructures involving 2D magnets fertile grounds for emergent interfacial phenomena.

Control of 2D magnetism

Electric control of low-dimensional magnetic systems (*82*, *83*), through either an electric field or electrostatic doping, changes the electron population, orbital occupation, and possibly electrochemical reactions (*84*), leading to the modification of exchange parameters and magnetic anisotropies and thus the resultant magnetic properties. Electrical control of recently emerged 2D magnets has been achieved. In bilayer antiferromagnetic CrI_3, both electric fields and electrostatic doping can affect the spin-flipping magnetic field (*85*–*87*). One remarkable phenomenon is the almost complete conversion of the few-layer graphene-encapsulated bilayer CrI_3 from interlayer antiferromagnetism to ferromagnetism by electrostatic doping (*87*). The Curie temperature of single-layer CrI_3 was modulated between 40 K and 50 K by changing doping levels. Electrical control of few-layer $Cr_2Ge_2Te_6$ via ionic liquid gating shows the modulation of coercivity and saturation field (*88*). In contrast to magnetic insulators, the itinerant nature of ferromagnetism in Fe_3GeTe_2, given the magnetism is mediated through conductive electrons, possibly allows more effective tuning of Curie temperatures by controlling the carrier concentrations within. The hysteresis loop of few-layer Fe_3GeTe_2 was recently reported in anomalous Hall effect measurements at room temperature (*62*), while the 2D magnet was electrostatically doped via an ionic liquid. Scanning microscopy may provide further information on whether a long-range ferromagnetic order or local magnetic islands are formed, considering that both structural distortion and electrochemical reaction possibly occur when 2D materials meet ionic liquids. Also, the conversion between antiferromagnetism and ferromagnetism was predicted to occur in both electron- and hole-doped $MnPSe_3$ above 3×10^{13} to 4×10^{13} carriers/cm^2 (*89*). Such antiferromagnetism-ferromagnetism conversion may prompt a new means of magnetization switching for logics and memories.

Magnetoelectric multiferroics could enhance the efficiency of electric control of magnetism because of the inherent coupling of magnetic and electric orders. Magnetoelectric multiferroics that simultaneously possess ferromagnetism and ferroelectricity hold great promise in next-generation spintronics and microwave magnetoelectric applications. However, in the 2D regime, each type of ferroic order has its own hindrance, such as the enhanced thermal fluctuations for 2D ferromagnetism and the strong depolarization fields for 2D ferroelectricity. Despite the recent success in realizing 2D ferromagnetism and 2D ferroelectricity (*90*–*94*) in different 2D materials, the simultaneous realization of both orders in one 2D material has not been reached. The theoretically predicted 2D multiferroics are primarily of ferromagnetism and ferroelasticity [e.g., monolayer group IV mono-oxide α-SnO (*95*)] and of ferroelectricity and ferroelasticity [e.g., monolayer group IV monochalcogenides such as GeS, GeSe, SnS, and SnSe (*96*) and monolayer ternary compounds such as GaTeCl (*97*)]. At the time of writing, very few theoretical predictions have been made on 2D magnetoelectric multiferroics (*98*, *99*). An unusual 2D magnetoelectric multiferroics was predicted on the basis of hyperferroelectric CrN (*98*). The scarcity of single-phase 2D magnetoelectric multiferroics relates to the long-standing challenge in multiferroics physics: Ferromagnetism prefers partially filled *d*-orbitals, whereas ferroelectricity prefers empty *d*-orbitals for displacive movement of ions.

Another knob for the effective control of magnetism is pressure or strain. Magnetic properties critically hinge on materials' structural parameters. Thus, spin-lattice coupling and magnetostrictions are common phenomena in magnetic materials. Spin-lattice coupling has been experimentally observed or theoretically predicted in layered magnets such as $Cr_2Si_2Te_6$ (*45*), $Cr_2Ge_2Te_6$ (*100*), and Fe_3GeTe_2 (*58*). While being cooled into ferromagnetic phase, both the in-plane lattice constant and the interlayer spacing of $Cr_2Si_2Te_6$ undergo the increase (*45*). For $Cr_2Ge_2Te_6$, frequencies of a few phonons exhibit upturns while being cooled into a ferromagnetic phase, highlighting the spin-phonon coupling (*100*). A hydrostatic pressure of 1 GPa can reduce the Curie temperature of the bulk $Cr_2Ge_2Te_6$ by ~9% (*101*). Furthermore, hydrostatic pressures above 1 GPa can reorient the spins of the bulk $Cr_2Ge_2Te_6$ from out-of-plane to in-plane (*102*). As discussed above, pressurized $FePSe_3$ even underwent a transformation from antiferromagnetic insulator to superconductor. These findings showcase the effectiveness of pressure or strain in engineering 2D magnets.

Heterostructures and interfacial engineering

High spin and valley polarizations in 2D materials provide tantalizing opportunities for efficient spintronics and valleytronics. Placing 2D electronic or valleytronic materials on magnetic insulators offers an effective methodology to spin-polarize and/or valley-polarize 2D materials. Especially if such magnetic insulators are also vdW materials, the seamless integration and interplay of vdW heterostructures could benefit the interfacial exchange interaction due to atomically sharp interfacial registry. Various material systems in which the proximity effect has been used to spin- or valley-polarize 2D materials include graphene on YIG (*40*), EuS on graphene (*41*), WSe_2 on EuS (*103*), and WSe_2 on CrI_3 (*104*).

Time-reversal symmetry breaking in 3D topological insulators can induce a gap opening in the 2D Dirac surface states, possibly giving rise to quantum anomalous Hall states on 1D edges. The conventional way to realize the quantum

anomalous Hall effect (QAHE) is through magnetic dopants, such as Cr-doped Bi_2Se_3. However, magnetic impurities scatter the electrons' traveling and suppress the temperature limit for the realization of QAHE. Given the atomically flat vdW ferromagnet, the sharp interfacial registry may effectively magnetize the surfaces of topological insulators without incurring structural perturbations. Such endeavors have been attempted using metal-organic chemical vapor deposition of Bi_2Te_3 on $Cr_2Ge_2Te_6$ (*105*) and MBE growth of $Cr_2Ge_2Te_6$ on $(Bi,Sb)_2Te_3$ (*106*). Another surge of interest toward QAHE was triggered by the recent advances in the synthesis of intrinsic magnetic topological insulators such as $MnBi_2Te_4$ and $MnBi_2Se_4$ (*107*–*112*). These layered materials are not only intrinsically magnetic but also topologically nontrivial. Rather than randomly distributing in the Bi sites substitutionally, Mn self-organizes in the center layer of the septuple layers of, for example, $Mn_2Bi_2Te_4$, which is an A-type antiferromagnetic topological insulator and may host the quantized topological magnetoelectric effect, quantum anomalous Hall state, and intrinsic axion insulator state. Successful synthesis of $Mn_2Bi_2Te_4$ in both thin films and millimeter-size bulk single crystals (*108*) has been reported.

Placing 2D vdW magnets in contact with other materials not only lends the magnetic properties of 2D magnets to others, but can also modify the 2D magnets via interfacial engineering. A remarkable example is the magnetic phase at the EuS-Bi_2Se_3 interface persisting beyond room temperature (*113*). Interfacial engineering represents a vital scheme to tailor 2D magnetic properties: It is based on artificial material systems, which means tremendous freedom relative to the design and synthesis of single-phase materials. Moreover, unlike the modulation of magnetic properties through external stimuli such as electrical field, interface engineering does not require external power sources to maintain the modified properties.

A host of factors make possible the interface engineering of 2D magnets, as summarized in Fig. 4:

1) The interface charge transfer changes the electron concentration and orbital occupation in 2D magnets, leading to the property change.

2) The interface dipole or built-in electric field can modify the electronic structure or crystal field of 2D magnets.

The above two factors were proposed to explain the nonzero remanent magnetization in bilayer CrI_3 sandwiched by few-layer graphene [figure 3a of (*87*)] and the different magnetic properties between graphite-bilayer CrI_3-BN and BN-bilayer CrI_3-BN [figure S4 of (*85*)]. The interface effects in the resultant 2D magnetic properties were also reflected by the distinct coercivities in different regions of the same monolayer CrI_3 flake sandwiched by graphite [figure 2d of (*15*)].

3) The interfacial orbital hybridization affects the resultant magnetic property of 2D magnets by impinging on the electronic properties and orbital characters of 2D magnets.

4) The morphology and lattice strain of 2D magnets can be modified when 2D magnets interface with other materials, resulting in the change of 2D magnetic properties.

5) Exchange anisotropy and the superexchange mediated by outermost atoms of 2D magnets are susceptible to the contacted materials.

6) The band structure of a 2D magnet may renormalize when interfacing with a material of a similar lattice constant. For example, graphene band properties can be strongly altered by *h*-BN. Band renormalization of 2D magnets can also be caused by the dielectric screening of adjacent materials.

7) The dielectric environments screen the coulombic interaction (note: in nature, exchange interaction is a coulombic interaction). Such dielectric screening of electron-electron interaction has been well studied for mobility enhancement in transistors (*114*) and has been shown to effectively weaken the excitonic binding energy in 2D materials [the adjacent single-side bilayer graphene reduces the excitonic binding energy in $MoSe_2$ by ~100 meV (*115*)].

8) The spin-orbit coupling proximity can play a role when 2D magnets are in contact with heavy elements, given that the magnetocrystalline anisotropy is intrinsically related to the spin-orbit coupling. For example, graphene's spin-orbit coupling strength was enhanced three orders of magnitude by contacting WS_2 (*116*).

Device applications: 2D spintronics, magnonics, and spin-orbitronics

The magnetic tunnel junction (MTJ) is a fundamental building block for the state-of-the-art spintronic industry (*7*, *8*, *117*–*123*). One of the obvious advantages in all-vdW MTJs is that the uniform barrier thickness facilitates the all-area tunneling. In contrast, tunneling in nonuniform MTJs preferentially occurs through thinner barrier regions, because the tunneling current is an exponential function of the barrier thickness. Such vdW MTJs have been pursued based on

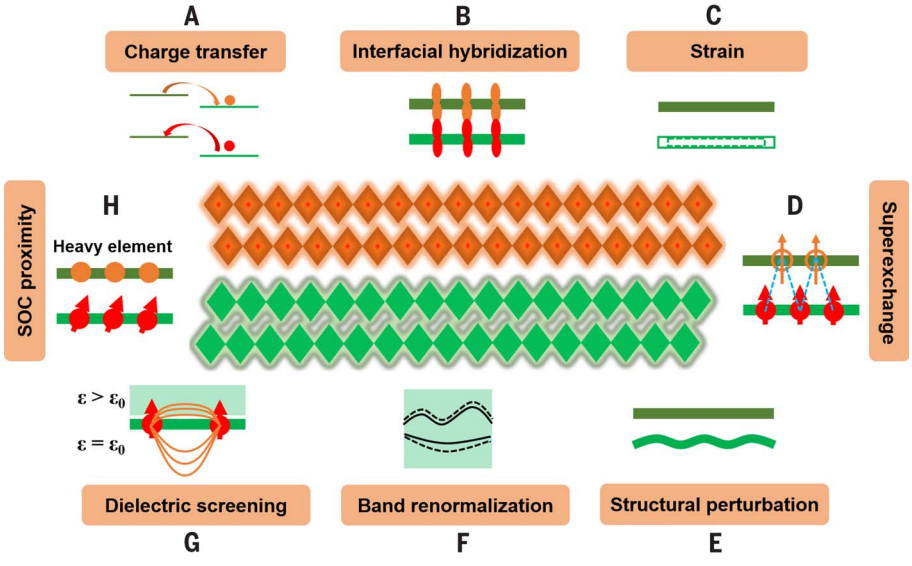

Fig. 4. Interfacial engineering of 2D magnets. Magnetic properties of 2D magnets can be affected by adjacent materials via different mechanisms. The central structure depicts an interface between a 2D magnet (green) and a dissimilar material (orange). (**A**) Charge transfer and interfacial dipole. The orange and red balls represent electrons and holes, respectively. (**B**) Interfacial hybridization. The lower green bar represents a 2D magnet; the upper bar is a dissimilar material. The dumbbells represent electronic orbitals of the two materials, overlapping at the interface to hybridize. (**C**) Strain effect. The lower solid bar represents a stretched 2D magnet in contact with a dissimilar material; the lower dashed bar represents the relaxed 2D magnet without the top contacted material. (**D**) Additional superexchange interactions. The orange circles with arrows represent the elements in adjacent materials that provide additional channels to mediate the superexchange interaction between magnetic ions in 2D magnets, which are represented by the red solid balls with arrows. (**E**) Structural perturbation. The wavy green belt represents 2D magnets that are structurally perturbed because of contact with the adjacent materials. (**F**) Band renormalization. The solid curves represent the electronic, magnonic, or phononic band dispersions of 2D magnets after band renormalization with contact of the adjacent materials; the dashed curves represent the same band dispersions before band renormalization without contacting the adjacent materials. (**G**) Dielectric screening. Red balls with arrows represent the exchange-coupled electrons in 2D magnets; orange curves depict the electric field lines connecting electrons. The environment with higher dielectric constant ε screens the coulombic interaction more. The nature of exchange interaction as a coulombic interaction makes 2D magnets susceptible to the dielectric screening. (**H**) Spin-orbit coupling (SOC) proximity. By contacting heavy-element materials, the SOC in 2D magnets will be effectively modified, leading to the change of magnetocrystalline anisotropy.

$Fe_{0.25}TaS_2$-Ta_2O_5-$Fe_{0.25}TaS_2$ (*124*), graphite-CrI_3-graphite (*49*, *125*–*127*), Fe_3GeTe_2-BN-Fe_3GeTe_2 (*128*), and graphite-$CrBr_3$-graphite (*129*). The Curie temperatures of Fe_xTaS_2 are tunable by Fe's stoichiometry with maximum T_C at ~160 K when $x = 0.2$, and Ta_2O_5 is a thin non-vdW native oxide (Fig. 5, A and B). The tunneling magnetoresistance is about 6.5% at 5 K (*124*). Recently, several research groups reported the very large tunneling magnetoresistance based on graphite-CrI_3-graphite sandwich structures (Fig. 5, C and D), with maximal magnetoresistance amounting to 19,000% at 2 K (*125*), 550% at 300 mK (*126*), 10,000% at 10 K (*49*), and 1,000,000% at 1.4 K (*127*). The large variance among these reported tunneling magnetoresistance values relates to such detailed experimental conditions as measurement temperature, thickness of the spacing layer, applied bias, and the detailed interfacial quality. The key of this type of MTJ was deemed to make use of the multiple scattering of tunneling electrons across the alternatively spin-polarized CrI_3 layers. These MTJs were found to be a result of the magnon-mediated tunneling process, in contrast to the conventional phonon- or electron-mediated tunneling (*126*, *129*). Another vdW MTJ, Fe_3GeTe_2-BN-Fe_3GeTe_2, exhibited 160% tunneling magnetoresistance at 4.2 K (*128*). These proof-of-concept studies show the attractive promise of vdW magnets in high-efficiency spintronics or magnonics.

To be balanced, outstanding challenges remain in these vdW MTJs concerning room temperature, nonvolatility, and low-power switching. For example, the current version of CrI_3-MTJs works at about liquid helium temperatures, is volatile, and requires large magnetic fields for toggling between distinct states (e.g., 2 T for tetralayers). For practical vdW MTJs, efforts need to be directed toward such important issues as high-temperature 2D magnets, perpendicular anisotropy, large remanence, modest coercivity, and robust exchange bias with antiferromagnets. Nonetheless, despite challenges, it is hoped that the smaller magnetic volume in ultrathin vdW MTJs, better electrical control, and enhanced thermal fluctuations in 2D magnets could allow a lower critical current for spin torque magnetization switching relative to the traditional non-vdW MTJs. This lower critical current is the key long-sought goal for spin-transfer torque magnetoresistive random-access memory (STT-MRAM).

Bilayer structures consisting of 2D and magnetic materials provide intriguing opportunities in magnonics and spin-orbitronics. Spin pumping and spin-orbit torque are reciprocal processes. Magnons can be excited in magnetic substrates coherently by microwave. The excited magnons, without the necessity of conducting electrons, then propagate into the adjacent 2D materials. If the 2D materials have large spin-orbit coupling strengths or large inverse Rashba-Edelstein coefficients, they would be capable of efficiently converting the traveling magnons into charge current and detectable voltage. Proof-of-concept experiments on such spin-charge conversion have been conducted in graphene-YIG (*130*, *131*) (Fig. 5E), MoS_2-Al-Co (*132*), and MoS_2-YIG (*133*) heterostructures.

In a reverse manner to spin pumping, spin-transfer torque or spin-orbit torque results from an injection of spin current from a 2D material into a magnetic thin-film substrate. A longitudinal charge current in a 2D material with strong spin-orbit coupling can deflect electrons of transverse spin orientations toward the directions normal to the bilayer interface, resulting in the injection of a

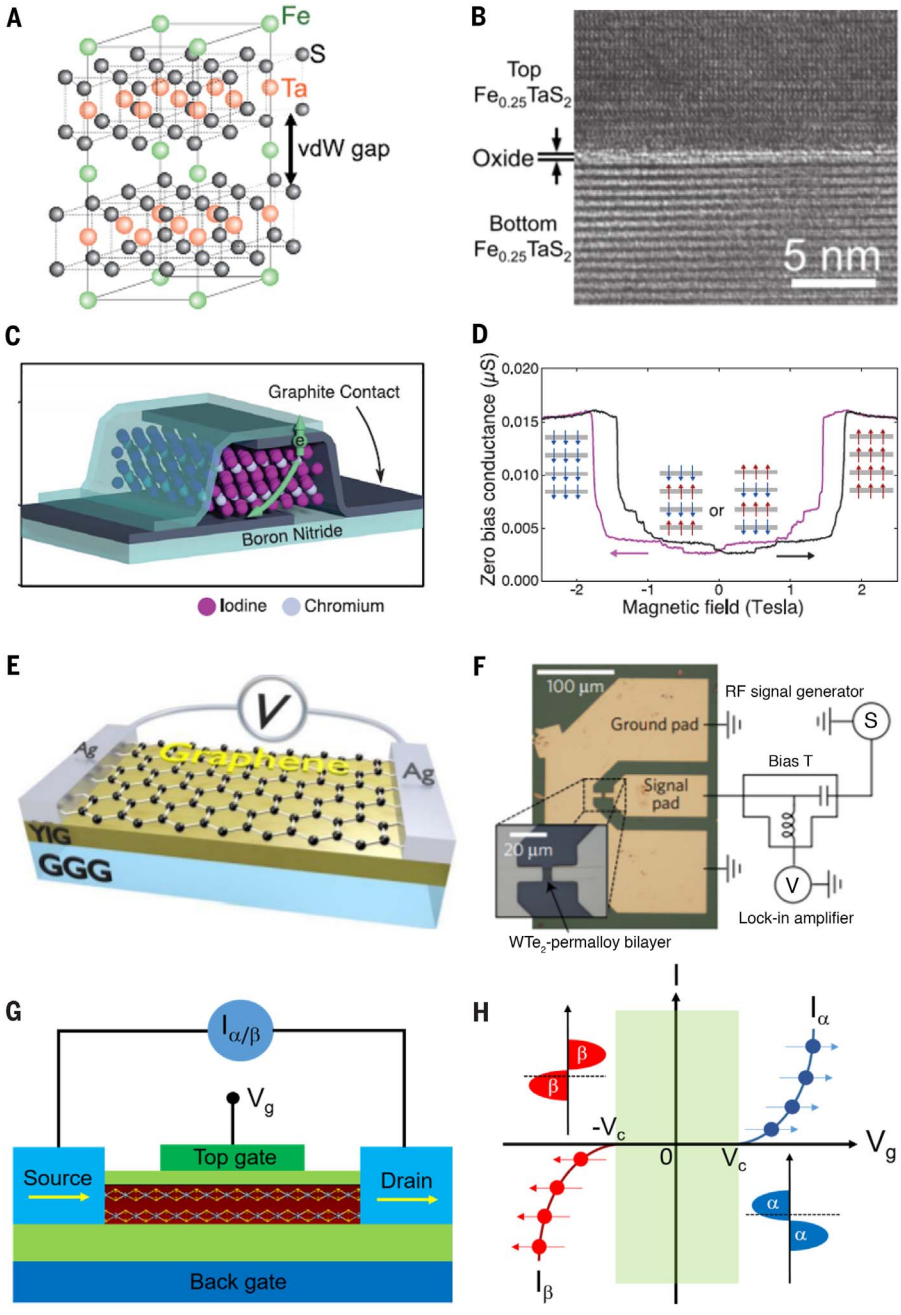

Fig. 5. Spintronic, magnonic, and spin-orbitronic devices based on 2D magnets or magnetic heterostructures. (**A** and **B**) MTJ based on $Fe_{0.25}TaS_2$-Ta_2O_5-$Fe_{0.25}TaS_2$ (*124*). Iron-intercalated TaS_2 is ferromagnetic, and the surface native oxide was used as an insulating spacing layer. (A) Atomic structure of Fe-intercalated TaS_2. (B) Cross-section transmission electron microscopy image of the MTJ sandwich structure. (**C** and **D**) MTJ based on graphite-CrI_3-graphite (*126*). (C) Schematic of MTJ. (D) Magnetic field–dependent tunneling conductance. (**E**) Schematic of graphene-YIG heterostructure for spin-charge conversion based on spin pumping (*130*). (**F**) Schematic of the spin-orbit torque measurement system, for which the core material architecture is WTe_2-permalloy heterostructure (*135*). Inset is an optical image of the tested device. (**G** and **H**) Schematics of a spin field-effect transistor based on a bilayer A-type antiferromagnet and its predicted electrical properties (*140*).

Chalcogenides	$Cr_2Ge_2Te_6$, $Cr_2Si_2Te_6$, Fe_3GeTe_2, VSe_2*, $MnSe_x$*	$Fe_2P_2S_6$, $Fe_2P_2Se_6$, $Mn_2P_2S_6$, $Mn_2P_2Se_6$, $Ni_2P_2S_6$, $Ni_2P_2Se_6$, $CuCrP_2Se_6$*, $AgVP_2S_6$, $AgCrP_2S_6$, $CrSe_2$, $CrTe_3$, $Ni_3Cr_2P_2S_9$, $MnBi_2Te_4$*, $MnBi_2Se_4$*	$CuCrP_2S_6$
Halides	CrI_3*, $CrBr_3$, GdI_2	$CrCl_3$, $FeCl_2$, $FeBr_2$, FeI_2, $MnBr_2$, $CoCl_2$, $CoBr_2$, $NiCl_2$, VCl_2, VBr_2, VI_2, $FeCl_3$, $FeBr_3$, CrOCl, CrOBr, CrSBr, $MnCl_2$*, VCl_3*, VBr_3*	$CuCl_2$, $CuBr_2$, $NiBr_2$, NiI_2, CoI_2, MnI_2 α-$RuCl_3$
Others	VS_2, InP_3, GaSe, GaS	MnX_3 (X = F, Cl, Br, I), FeX_2 (X = Cl, Br, I), MnSSe, $TiCl_3$, VCl_3	SnO, GeS, GeSe, SnS, SnSe, GaTeCl, CrN, CrB_2

Fig. 6. Van der Waals magnets library. Color code: Green, bulk ferromagnetic vdW crystals; orange, bulk antiferromagnets; yellow, bulk multiferroics; gray, theoretically predicted vdW ferromagnets (left), half metals (center), and multiferroics (right), which have not yet been experimentally confirmed; purple, α-$RuCl_3$ (a proximate Kitaev quantum spin liquid) (*144*). Notes (asterisks): VSe_2 has been found only in 1T-VSe_2 form in experiments to date (*145*), although the magnetic properties of 2H-VSe_2 have been widely studied by density functional theory calculations. $MnSe_x$ is ferromagnetic and of vdW structure in MBE-synthesized 2D form but is antiferromagnetic in bulk (which could be either rock-salt or hexagonal structure). CrI_3, although ferromagnetic in bulk, was experimentally suggested to be an A-type antiferromagnet in the 2D regime. $CuCrP_2Se_6$ does not host the electric order while being cooled down to 10 K according to experimental data (*147*), but the calculated ground state of $CuCrP_2Se_6$ is multiferroic with antiferroelectricity (*99*). $MnBi_2Te_4$ and $MnBi_2Se_4$ may exhibit ferrimagnetic features as a result of uncompensated odd-layer A-type antiferromagnets or surfaces of antiferromagnetic topological insulators. $MnCl_2$ has a magnetic structure that has not been completely determined, which could be either antiferromagnetic or helimagnetic (*142*). Bulk VCl_3 and VBr_3 have been inferred to be weak antiferromagnets on the basis of experimental data, although detailed magnetic structures have not been determined; however, monolayer VCl_3 was calculated to be ferromagnetic (*146*).

spin-polarized current into the magnetic substrate. The injected spin current exerts spin-orbit torques on the magnetic moments of the underlying magnetic substrate, exciting the moments to precess or even switch to the opposite orientation. Spin-orbit torque MRAM, if using 2D materials as the spin-current sources, has the potential toward the atomic thinness. The other advantage of using 2D materials as a spin-current source is that the majority of the spin current would be at the interface rather than being dissipated in bulk, constituting a tantalizing platform for low-power spintronics. Many types of bilayer structures consisting of 2D materials such as MoS_2-permalloy (*134*), WTe_2-permalloy (*135*) (Fig. 5F), and (MoS_2 and WSe_2)-CoFeB (*136*) have been investigated.

Lastly, it is worthwhile to note the family of half metals. To improve spintronics, high spin polarization at the Fermi level of a material is desirable. Half metallicity, a property arising from the metallic nature for electrons with singular spin polarization and insulating for electrons with the opposite spin, holds the potential for 100% spin-polarized conduction electrons. There have been a few theoretical predictions on the possible 2D half metals, including manganese trihalides (*137*), $FeCl_2$, $FeBr_2$, FeI_2 (*138*), and Janus structure of monolayer MnSSe (*139*). Half metallicity could also be electrically induced in bilayer A-type antiferromagnets (e.g., in 2H-VSe_2) (*140*). This electrically induced half metallicity potentially prompts a new type of spin–field-effect transistor in which both switching and reversal of spin polarization can be realized by a single knob: gate voltage, in analogy to the conventional semiconductor transistors (Fig. 5, G and H).

Conclusions and outlook

The recently discovered 2D magnetic crystals provide ideal platforms to study the ground state, fundamental excitations, dynamics, and frustrations of spin ensembles under strong quantum confinement. Such intrinsic 2D magnetic crystals distinguish themselves from traditional magnetic thin films and nonmagnetic 2D materials, in terms of both properties and application prospects. The interplay of dimensionality, correlation, charge, orbital character, and topology makes 2D magnetic crystals and heterostructures extremely fertile condensed matter systems with a large reservoir of exotic properties. The 2D materials' outstanding feature of being susceptible to a large variety of external stimuli makes the versatile control of 2D magnetism possible by electrical, mechanical, chemical, and optical approaches. Furthermore, because of the unrivaled compatibility for heterostructure constructions, vdW heterostructures present attractive opportunities for designer 2D magnetic, magnetoelectric, and magneto-optical artificial heteromaterials. Those materials that contact 2D magnets will affect the 2D magnetic properties. Novel spintronic, magnonic, and spin-orbitronic devices have started to emerge.

As evident in Fig. 6, a large variety of magnetic vdW materials are available (*141*–*148*), most of whose 2D counterparts remain to be studied. The family of 2D magnetic crystals is rapidly growing, magnetic heterostructures consisting of 2D materials are being actively expanded, and new device concepts are being developed. One of the most critical needs concerns the material-level realization of room-temperature 2D ferromagnets (in contrast to sustaining a high Curie temperature with external supplies such as electrical, optical, and mechanical means), which ideally would be air-stable. Furthermore, the wafer-scale synthesis (*149*) of such crystals has to be accomplished for practical mass production. Advances in both metallic and insulating 2D magnets, both 2D ferromagnets and antiferromagnets, promise various aspects of applications based on their distinct properties.

Fundamental spintronic parameters—including spin Hall angle, spin diffusion length, magnon damping coefficient, spin injection efficiency, and spin mixing conductance—must be evaluated in 2D magnets and across interfaces. There is a need for in-depth understanding of the relation between spintronic transport metrics and material parameters, along with the corresponding strategies for optimization. Furthermore, exotic spin textures and topologically protected spin configurations (e.g., magnetic skyrmions) in 2D magnets or heterostructures remain open to explore by rationally weighing the material constituents, crystal symmetry, spin-orbit coupling, Rashba effect, and spin (re-)orientations. New quantum phases and quasiparticles could be found, leading to new ways of computation and communication. Such advances in understanding and control of 2D magnetic crystals and emergent heterostructure devices will foster a widespread range of applications (*150*) including low-power spintronics, quantum computing, and optical communications.

REFERENCES AND NOTES

1. P. Weiss, L'Hypothèse du champ moléculaire et la propriété ferromagnétique. *J. Phys. Theor. Appl.* **6**, 661–690 (1907). doi: 10.1051/jphystap:019070060066100
2. W. Heisenberg, Mehrkörperproblem und Resonanz in der Quantenmechanik. *Z. Phys.* **38**, 411–426 (1926). doi: 10.1007/BF01397160
3. P. A. M. Dirac, On the theory of quantum mechanics. *Proc. R. Soc. London Ser. A* **112**, 661–677 (1926). doi: 10.1098/rspa.1926.0133
4. N. D. Mermin, H. Wagner, Absence of ferromagnetism or antiferromagnetism in one- or two-dimensional isotropic Heisenberg models. *Phys. Rev. Lett.* **17**, 1133–1136 (1966). doi: 10.1103/PhysRevLett.17.1133
5. P. Bruno, Magnetization and Curie temperature of ferromagnetic ultrathin films: The influence of magnetic anisotropy and dipolar interactions. *Proc. MRS* **231**, 299–310 (1991). doi: 10.1557/PROC-231-299
6. C. Gong *et al.*, Discovery of intrinsic ferromagnetism in two-dimensional van der Waals crystals. *Nature* **546**, 265–269 (2017). doi: 10.1038/nature22060; pmid: 28445468
7. M. N. Baibich *et al.*, Giant magnetoresistance of (001)Fe/(001)Cr magnetic superlattices. *Phys. Rev. Lett.* **61**, 2472–2475 (1988). doi: 10.1103/PhysRevLett.61.2472; pmid: 10039127

8. G. Binasch, P. Grünberg, F. Saurenbach, W. Zinn, Enhanced magnetoresistance in layered magnetic structures with antiferromagnetic interlayer exchange. *Phys. Rev. B* **39**, 4828–4830 (1989). doi: 10.1103/PhysRevB.39.4828; pmid: 9948867
9. Y. Li, K. Baberschke, Dimensional crossover in ultrathin Ni(111) films on W(110). *Phys. Rev. Lett.* **68**, 1208–1211 (1992). doi: 10.1103/PhysRevLett.68.1208; pmid: 10046107
10. Z. Q. Qiu, J. Pearson, S. D. Bader, Magnetic phase transition of ultrathin Fe films on Ag(111). *Phys. Rev. Lett.* **67**, 1646–1649 (1991). doi: 10.1103/PhysRevLett.67.1646;pmid: 10044208
11. C. H. Back *et al*., Experimental confirmation of universality for a phase transition in two dimensions. *Nature* **378**, 597–600 (1995). doi: 10.1038/378597a0
12. S. S. P. Parkin, N. More, K. P. Roche, Oscillations in exchange coupling and magnetoresistance in metallic superlattice structures: Co/Ru, Co/Cr, and Fe/Cr. *Phys. Rev. Lett.* **64**, 2304–2307 (1990). doi: 10.1103/PhysRevLett.64.2304; pmid: 10041640
13. L. M. Falicov *et al*., Surface, interface, and thin-film magnetism. *J. Mater. Res.* **5**, 1299–1340 (1990). doi: 10.1557/JMR.1990.1299
14. H. C. Siegmann, Surface and 2D magnetism. *J. Phys. Condens. Matter* **4**, 8395–8434 (1992). doi: 10.1088/0953-8984/4/44/004
15. B. Huang *et al*., Layer-dependent ferromagnetism in a van der Waals crystal down to the monolayer limit. *Nature* **546**, 270–273 (2017). doi: 10.1038/nature22391; pmid: 28593970
16. O. V. Yazyev, L. Helm, Defect-induced magnetism in graphene. *Phys. Rev. B* **75**, 125408 (2007). doi: 10.1103/PhysRevB.75.125408
17. M. M. Ugeda, I. Brihuega, F. Guinea, J. M. Gómez-Rodríguez, Missing atom as a source of carbon magnetism. *Phys. Rev. Lett.* **104**, 096804 (2010). doi: 10.1103/PhysRevLett.104.096804; pmid: 20367003
18. H. González-Herrero *et al*., Atomic-scale control of graphene magnetism by using hydrogen atoms. *Science* **352**, 437–441 (2016). doi: 10.1126/science.aad8038; pmid: 27102478
19. R. R. Nair *et al*., Dual origin of defect magnetism in graphene and its reversible switching by molecular doping. *Nat. Commun.* **4**, 2010 (2013). doi: 10.1038/ncomms3010; pmid: 23760522
20. J. Cervenka, M. I. Katsnelson, C. F. J. Flipse, Room-temperature ferromagnetism in graphite driven by two-dimensional networks of point defects. *Nat. Phys.* **5**, 840–844 (2009). doi: 10.1038/nphys1399
21. B. Uchoa, V. N. Kotov, N. M. R. Peres, A. H. Castro Neto, Localized magnetic states in graphene. *Phys. Rev. Lett.* **101**, 026805 (2008). doi: 10.1103/PhysRevLett.101.026805; pmid: 18764214
22. K. M. McCreary, A. G. Swartz, W. Han, J. Fabian, R. K. Kawakami, Magnetic moment formation in graphene detected by scattering of pure spin currents. *Phys. Rev. Lett.* **109**, 186604 (2012). doi: 10.1103/PhysRevLett.109.186604; pmid: 23215308
23. R. R. Nair *et al*., Spin-half paramagnetism in graphene induced by point defects. *Nat. Phys.* **8**, 199–202 (2012). doi: 10.1038/nphys2183
24. M. Sepioni, R. R. Nair, I.-L. Tsai, A. K. Geim, I. V. Grigorieva, Revealing common artifacts due to ferromagnetic inclusions in highly oriented pyrolytic graphite. *EPL* **97**, 47001 (2012). doi: 10.1209/0295-5075/97/47001
25. M. Sepioni *et al*., Limits on intrinsic magnetism in graphene. *Phys. Rev. Lett.* **105**, 207205 (2010). doi: 10.1103/PhysRevLett.105.207205; pmid: 21231263
26. O. V. Yazyev, M. I. Katsnelson, Magnetic correlations at graphene edges: Basis for novel spintronics devices. *Phys. Rev. Lett.* **100**, 047209 (2008). doi: 10.1103/PhysRevLett.100.047209; pmid: 18352331
27. J. Jung, T. Pereg-Barnea, A. H. Macdonald, Theory of interedge superexchange in zigzag edge magnetism. *Phys. Rev. Lett.* **102**, 227205 (2009). doi: 10.1103/PhysRevLett.102.227205; pmid: 19658901
28. Y. W. Son, M. L. Cohen, S. G. Louie, Half-metallic graphene nanoribbons. *Nature* **444**, 347–349 (2006). doi: 10.1038/nature05180; pmid: 17108960
29. P. Gambardella *et al*., Ferromagnetism in one-dimensional monatomic metal chains. *Nature* **416**, 301–304 (2002). doi: 10.1038/416301a; pmid: 11907571
30. G. Z. Magda *et al*., Room-temperature magnetic order on zigzag edges of narrow graphene nanoribbons. *Nature* **514**, 608–611 (2014). doi: 10.1038/nature13831; pmid: 25355361
31. M. Slota *et al*., Magnetic edge states and coherent manipulation of graphene nanoribbons. *Nature* **557**, 691–695 (2018). doi: 10.1038/s41586-018-0154-7; pmid: 29849157
32. O. V. Yazyev, Emergence of magnetism in graphene materials and nanostructures. *Rep. Prog. Phys.* **73**, 056501 (2010). doi: 10.1088/0034-4885/73/5/056501
33. D. Pesin, A. H. MacDonald, Spintronics and pseudospintronics in graphene and topological insulators. *Nat. Mater.* **11**, 409–416 (2012). doi: 10.1038/nmat3305; pmid: 22522641
34. T. Stauber, N. M. R. Peres, F. Guinea, A. H. Castro Neto, Fermi liquid theory of a Fermi ring. *Phys. Rev. B* **75**, 115425 (2007). doi: 10.1103/PhysRevB.75.115425
35. E. V. Castro, N. M. R. Peres, T. Stauber, N. A. P. Silva, Low-density ferromagnetism in biased bilayer graphene. *Phys. Rev. Lett.* **100**, 186803 (2008). doi: 10.1103/PhysRevLett.100.186803; pmid: 18518403
36. T. Cao, Z. Li, S. G. Louie, Tunable magnetism and half-metallicity in hole-doped monolayer GaSe. *Phys. Rev. Lett.* **114**, 236602 (2015). doi: 10.1103/PhysRevLett.114.236602; pmid: 26196815
37. S. Wu, X. Dai, H. Yu, H. Fan, J. Hu, W. Yao, Magnetism in p-type monolayer gallium chalcogenides (GaSe, GaS). arXiv:1409.4733 [cond-mat.mes-hall] (17 September 2014).
38. W. L. Bloss, L. J. Sham, V. Vinter, Interaction-induced transition at low densities in silicon inversion layer. *Phys. Rev. Lett.* **43**, 1529–1532 (1979). doi: 10.1103/PhysRevLett.43.1529
39. P. Back *et al*., Giant paramagnetism-induced valley polarization of electrons in charge-tunable monolayer $MoSe_2$. *Phys. Rev. Lett.* **118**, 237404 (2017). doi: 10.1103/PhysRevLett.118.237404; pmid: 28644665
40. Z. Wang, C. Tang, R. Sachs, Y. Barlas, J. Shi, Proximity-induced ferromagnetism in graphene revealed by the anomalous Hall effect. *Phys. Rev. Lett.* **114**, 016603 (2015). doi: 10.1103/PhysRevLett.114.016603; pmid: 25615490
41. P. Wei *et al*., Strong interfacial exchange field in the graphene/EuS heterostructure. *Nat. Mater.* **15**, 711–716 (2016). doi: 10.1038/nmat4603; pmid: 27019382
42. D. Maryenko *et al*., Observation of anomalous Hall effect in a non-magnetic two-dimensional electron system. *Nat. Commun.* **8**, 14777 (2017). doi: 10.1038/ncomms14777; pmid: 28300133
43. J. C. Leutenantsmeyer, A. A. Kaverzin, M. Wojtaszek, B. J. van Wees, Proximity induced room temperature ferromagnetism in graphene probed with spin currents. *2D Mater.* **4**, 014001 (2017). doi: 10.1088/2053-1583/4/1/014001
44. S. Singh *et al*., Strong modulation of spin currents in bilayer graphene by static and fluctuating proximity exchange fields. *Phys. Rev. Lett.* **118**, 187201 (2017). doi: 10.1103/PhysRevLett.118.187201; pmid: 28524685
45. L. D. Casto *et al*., Strong spin-lattice coupling in $CrSiTe_3$. *APL Mater.* **3**, 041515 (2015). doi: 10.1063/1.4914134
46. H. L. Zhuang, Y. Xie, P. R. C. Kent, P. Ganesh, Computational discovery of ferromagnetic semiconducting single-layer $CrSnTe_3$. *Phys. Rev. B* **92**, 035407 (2015). doi: 10.1103/PhysRevB.92.035407
47. J. L. Lado, J. Fernández-Rossier, On the origin of magnetic anisotropy in two dimensional CrI_3. *2D Mater.* **4**, 035002 (2017). doi: 10.1088/2053-1583/aa75ed
48. M. A. McGuire, H. Dixit, V. R. Cooper, B. C. Sales, Coupling of crystal structure and magnetism in the layered, ferromagnetic insulator CrI_3. *Chem. Mater.* **27**, 612–620 (2015). doi: 10.1021/cm504242t
49. Z. Wang *et al*., Very large tunneling magnetoresistance in layered magnetic semiconductor CrI_3. *Nat. Commun.* **9**, 2516 (2018). doi: 10.1038/s41467-018-04953-8; pmid: 29955066
50. P. Jiang, C. Wang, D. Chen, Z. Zhong, Z. Yuan, Z.-Y. Lu, W. Ji, Stacking tunable interlayer magnetism in bilayer CrI_3. arXiv:1806. 09274 [cond-mat.mtrl-sci] (25 June 2018).
51. D. Soriano, C. Cardoso, J. Fernández-Rossier, Interplay between interlayer exchange and stacking in CrI_3 bilayers. arXiv:1807.00357 [cond-mat.mes-hall] (1 July 2018).
52. N. Sivadas, S. Okamoto, X. Xu, C. J. Fennie, D. Xiao, Stacking-dependent magnetism in bilayer CrI_3. arXiv:1808.06559 [cond-mat.mtrl-sci] (15 November 2018).
53. D. Shcherbakov *et al*., Raman spectroscopy, photocatalytic degradation, and stabilization of atomically thin chromium tri-iodide. *Nano Lett.* **18**, 4214–4219 (2018). doi: 10.1021/acs.nanolett.8b01131; pmid: 29863369
54. M. Abramchuk *et al*., Controlling magnetic and optical properties of the van der Waals crystal $CrCl_{3-x}Br_x$ via mixed halide chemistry. *Adv. Mater.* **30**, 1801325 (2018). doi: 10.1002/adma.201801325; pmid: 29719069
55. H. J. Deiseroth, K. Aleksandrov, C. Reiner, L. Kienle, R. K. Kremer, Fe_3GeTe_2 and Ni_3GeTe_2 - two new layered transition-metal compounds: Crystal structures, HRTEM investigations, and magnetic and electrical properties. *Eur. J. Inorg. Chem.* **2006**, 1561–1567 (2006). doi: 10.1002/ejic.200501020
56. B. Chen *et al*., Magnetic properties of layered itinerant electron ferromagnet Fe_3GeTe_2. *J. Phys. Soc. Jpn.* **82**, 124711 (2013). doi: 10.7566/JPSJ.82.124711
57. J.-X. Zhu *et al*., Electronic correlation and magnetism in the ferromagnetic metal Fe_3GeTe_2. *Phys. Rev. B* **93**, 144404 (2016). doi: 10.1103/PhysRevB.93.144404
58. H. L. Zhuang, P. R. C. Kent, R. G. Hennig, Strong anisotropy and magnetostriction in the two-dimensional Stoner ferromagnet Fe_3GeTe_2. *Phys. Rev. B* **93**, 134407 (2016). doi: 10.1103/PhysRevB.93.134407
59. A. F. May, S. Calder, C. Cantoni, H. Cao, M. A. McGuire, Magnetic structure and phase stability of the van der Waals bonded ferromagnet $Fe_{3-x}GeTe_2$. *Phys. Rev. B* **93**, 014411 (2016). doi: 10.1103/PhysRevB.93.014411
60. J. Yi *et al*., Competing antiferromagnetism in a quasi-2D itinerant ferromagnet: Fe_3GeTe_2. *2D Mater.* **4**, 011005 (2017). doi: 10.1088/2053-1583/4/1/011005
61. Y. Zhang *et al*., Emergence of Kondo lattice behavior in a van der Waals itinerant ferromagnet, Fe_3GeTe_2. *Sci. Adv.* **4**, eaao6791 (2018). doi: 10.1126/sciadv.aao6791
62. Y. Deng *et al*., Gate-tunable room-temperature ferromagnetism in two-dimensional Fe_3GeTe_2. *Nature* **563**, 94–99 (2018). doi: 10.1038/s41586-018-0626-9; pmid: 30349002
63. Z. Fei *et al*., Two-dimensional itinerant ferromagnetism in atomically thin Fe_3GeTe_2. *Nat. Mater.* **17**, 778–782 (2018). doi: 10.1038/s41563-018-0149-7; pmid: 30104669
64. C. Tan *et al*., Hard magnetic properties in nanoflake van der Waals Fe_3GeTe_2. *Nat. Commun.* **9**, 1554 (2018). doi: 10.1038/s41467-018-04018-w; pmid: 29674662
65. G. D. Nguyen *et al*., Visualization and manipulation of magnetic domains in the quasi-two-dimensional material Fe_3GeTe_2. *Phys. Rev. B* **97**, 014425 (2018). doi: 10.1103/PhysRevB.97.014425
66. Q. Li *et al*., Patterning-induced ferromagnetism of Fe_3GeTe_2 van der Waals materials beyond room temperature. *Nano Lett.* **18**, 5974–5980 (2018). doi: 10.1021/acs.nanolett.8b02806; pmid: 30114354
67. T. Jungwirth, X. Marti, P. Wadley, J. Wunderlich, Antiferromagnetic spintronics. *Nat. Nanotechnol.* **11**, 231–241 (2016). doi: 10.1038/nnano.2016.18; pmid: 26936817
68. P. Wadley *et al*., Electrical switching of an antiferromagnet. *Science* **351**, 587–590 (2016). doi: 10.1126/science.aab1031; pmid: 26841431
69. V. W. Klingen, G. Eulenberger, H. Hahn, Uber die Kristallstrukturen von $Fe_2P_2Se_6$ und $Fe_2P_2S_6$. *Z. Anorg. Allg. Chem.* **401**, 97–112 (1973). doi: 10.1002/zaac.19734010113
70. A. R. Wildes, K. C. Rule, R. I. Bewley, M. Enderle, T. J. Hicks, The magnon dynamics and spin exchange parameters of $FePS_3$. *J. Phys. Condens. Matter* **24**, 416004 (2012). doi: 10.1088/0953-8984/24/41/416004; pmid: 23006615
71. B. Taylor, J. Steger, A. Wold, E. Kostiner, Preparation and properties of iron phosphorus triselenide, $FePSe_3$. *Inorg. Chem.* **13**, 2719–2721 (1974). doi: 10.1021/ic50141a034
72. A. Wiedenmann, J. Rossat-Mignod, A. Louisy, R. Brec, J. Rouxel, Neutron diffraction study of the layered compounds $MnPSe_3$ and $FePSe_3$. *Solid State Commun.* **40**, 1067–1072 (1981). doi: 10.1016/0038-1098(81)90253-2
73. P. A. Joy, S. Vasudevan, Magnetism in the layered transition-metal thiophosphates MPS_3 (M=Mn, Fe, and Ni). *Phys. Rev. B* **46**, 5425–5433 (1992). doi: 10.1103/PhysRevB.46.5425; pmid: 10004324
74. J.-U. Lee *et al*., Ising-type magnetic ordering in atomically thin $FePS_3$. *Nano Lett.* **16**, 7433–7438 (2016). doi: 10.1021/acs.nanolett.6b03052; pmid: 27960508
75. M. Bonilla *et al*., Strong room-temperature ferromagnetism in VSe_2 monolayers on van der Waals substrates. *Nat. Nanotechnol.* **13**, 289–293 (2018). doi: 10.1038/s41565-018-0063-9; pmid: 29459653
76. D. J. O'Hara *et al*., Room temperature intrinsic ferromagnetism in epitaxial manganese selenide films in the monolayer limit. *Nano Lett.* **18**, 3125–3131 (2018). doi: 10.1021/acs.nanolett.8b00683; pmid: 29608316
77. R. J. Pollard, V. H. McCann, J. B. Ward, Magnetic structures of α-MnS and MnSe from ^{57}Fe Mossbauer spectroscopy. *J. Phys. C* **16**, 345–353 (1983). doi: 10.1088/0022-3719/16/2/017

78. D. J. O'Hara, T. Zhu, R. K. Kawakami, Importance of paramagnetic background subtraction for determining the magnetic moment in epitaxially grown monolayer and few-layer van der Waals magnets. *IEEE Magn. Lett.* **9**, 1405805 (2018). doi: 10.1109/LMAG.2018.2867339
79. S. Y. Kim *et al*., Charge-spin correlation in van der Waals antiferromagnet $NiPS_3$. *Phys. Rev. Lett.* **120**, 136402 (2018). doi: 10.1103/PhysRevLett.120.136402; pmid: 29694193
80. Y. Wang *et al*., Emergent superconductivity in an iron-based honeycomb lattice initiated by pressure-driven spin-crossover. *Nat. Commun.* **9**, 1914 (2018). doi: 10.1038/s41467-018-04326-1; pmid: 29765049
81. X. Zhang *et al*., Magnetic anisotropy of the single-crystalline ferromagnetic insulator $Cr_2Ge_2Te_6$. *Jpn. J. Appl. Phys.* **55**, 033001 (2016). doi: 10.7567/JJAP.55.033001
82. H. Ohno *et al*., Electric-field control of ferromagnetism. *Nature* **408**, 944–946 (2000). doi: 10.1038/35050040; pmid: 11140674
83. F. Matsukura, Y. Tokura, H. Ohno, Control of magnetism by electric fields. *Nat. Nanotechnol.* **10**, 209–220 (2015). doi: 10.1038/nnano.2015.22; pmid: 25740132
84. C. Bi *et al*., Reversible control of Co magnetism by voltage-induced oxidation. *Phys. Rev. Lett.* **113**, 267202 (2014). doi: 10.1103/PhysRevLett.113.267202; pmid: 25615378
85. S. Jiang, J. Shan, K. F. Mak, Electric-field switching of two-dimensional van der Waals magnets. *Nat. Mater.* **17**, 406–410 (2018). doi: 10.1038/s41563-018-0040-6; pmid: 29531370
86. B. Huang *et al*., Electrical control of 2D magnetism in bilayer CrI_3. *Nat. Nanotechnol.* **13**, 544–548 (2018). doi: 10.1038/s41565-018-0121-3; pmid: 29686292
87. S. Jiang, L. Li, Z. Wang, K. F. Mak, J. Shan, Controlling magnetism in 2D CrI_3 by electrostatic doping. *Nat. Nanotechnol.* **13**, 549–553 (2018). doi: 10.1038/s41565-018-0135-x; pmid: 29736035
88. Z. Wang *et al*., Electric-field control of magnetism in a few-layered van der Waals ferromagnetic semiconductor. *Nat. Nanotechnol.* **13**, 554–559 (2018). doi: 10.1038/s41565-018-0186-z; pmid: 29967458
89. X. Li, X. Wu, J. Yang, Half-metallicity in $MnPSe_3$ exfoliated nanosheet with carrier doping. *J. Am. Chem. Soc.* **136**, 11065–11069 (2014). doi: 10.1021/ja505097m; pmid: 25036853
90. F. Liu *et al*., Room-temperature ferroelectricity in $CuInP_2S_6$ ultrathin flakes. *Nat. Commun.* **7**, 12357 (2016). doi: 10.1038/ncomms12357; pmid: 27510418
91. W. Ding *et al*., Prediction of intrinsic two-dimensional ferroelectrics in In_2Se_3 and other III_2-VI_3 van der Waals materials. *Nat. Commun.* **8**, 14956 (2017). doi: 10.1038/ncomms14956; pmid: 28387225
92. Y. Zhou *et al*., Out-of-plane piezoelectricity and ferroelectricity in layered α-In_2Se_3 nanoflakes. *Nano Lett.* **17**, 5508–5513 (2017). doi: 10.1021/acs.nanolett.7b02198; pmid: 28841328
93. C. Cui *et al*., Intercorrelated in-plane and out-of-plane ferroelecricity in ultrathin two-dimensional layered semiconductor In_2Se_3. *Nano Lett.* **18**, 1253–1258 (2018). doi: 10.1021/acs.nanolett.7b04852; pmid: 29378142
94. J. Xiao *et al*., Intrinsic two-dimensional ferroelectricity with dipole locking. *Phys. Rev. Lett.* **120**, 227601 (2018). doi: 10.1103/PhysRevLett.120.227601; pmid: 29906143
95. L. Seixas, A. S. Rodin, A. Carvalho, A. H. Castro Neto, Multiferroic two-dimensional materials. *Phys. Rev. Lett.* **116**, 206803 (2016). doi: 10.1103/PhysRevLett.116.206803; pmid: 27258881
96. H. Wang, X. Qian, Two-dimensional multiferroics in monolayer group IV monochalcogenides. *2D Mater.* **4**, 015042 (2017). doi: 10.1088/2053-1583/4/1/015042
97. S.-H. Zhang, B.-G. Liu, A controllable robust multiferroic GaTeCl monolayer with colossal 2D ferroelectricity and desirable multifunctionality. *Nanoscale* **10**, 5990–5996 (2018). doi: 10.1039/C7NR09588K; pmid: 29542759
98. W. Luo, K. Xu, H. Xiang, Two-dimensional hyperferroelectric metals: A different route to ferromagnetic-ferroelectric multiferroics. *Phys. Rev. B* **96**, 235415 (2017). doi: 10.1103/PhysRevB.96.235415
99. J. Qi, H. Wang, X. Chen, X. Qian, Two-dimensional multiferroic semiconductors with coexisting ferroelectricity and ferromagnetism. *Appl. Phys. Lett.* **113**, 043102 (2018). doi: 10.1063/1.5038037
100. Y. Tian, M. J. Gray, H. Ji, R. J. Cava, K. S. Burch, Magneto-elastic coupling in a potential ferromagnetic 2D atomic crystal. *2D Mater.* **3**, 025035 (2016). doi: 10.1088/2053-1583/3/2/025035
101. Y. Sun *et al*., Effects of hydrostatic pressure on spin-lattice coupling in two-dimensional ferromagnetic $Cr_2Ge_2Te_6$. *Appl. Phys. Lett.* **112**, 072409 (2018). doi: 10.1063/1.5016568
102. Z. Lin *et al*., Pressure-induced spin reorientation transition in layered ferromagnetic insulator $Cr_2Ge_2Te_6$. *Phys. Rev. Mater.* **2**, 051004 (2018). doi: 10.1103/PhysRevMaterials.2.051004
103. C. Zhao *et al*., Enhanced valley splitting in monolayer WSe_2 due to magnetic exchange field. *Nat. Nanotechnol.* **12**, 757–762 (2017). doi: 10.1038/nnano.2017.68; pmid: 28459469
104. D. Zhong *et al*., Van der Waals engineering of ferromagnetic semiconductor heterostructures for spin and valleytronics. *Sci. Adv.* **3**, e1603113 (2017). doi: 10.1126/sciadv.1603113; pmid: 28580423
105. L. D. Alegria *et al*., Large anomalous Hall effect in ferromagnetic insulator-topological insulator heterostructures. *Appl. Phys. Lett.* **105**, 053512 (2014). doi: 10.1063/1.4892353
106. M. Mogi *et al*., Ferromagnetic insulator $Cr_2Ge_2Te_6$ thin films with perpendicular remanence. *APL Mater.* **6**, 091104 (2018). doi: 10.1063/1.5046166
107. Y. Gong *et al*., Experimental realization of an intrinsic magnetic topological insulator. arXiv:1809.07926 [cond-mat.mtrl-sci] (21 September 2018).
108. M. M. Otrokov *et al*., Prediction and observation of the first antiferromagnetic topological insulator. arXiv:1809.07389 [cond-mat.mtrl-sci] (19 September 2018).
109. E. D. L. Rienks *et al*., Large magnetic gap at the Dirac point in a Mn-induced Bi_2Te_3 heterostructure. arXiv:1810.06238 [cond-mat.mtrl-sci] (15 October 2018).
110. J. Li *et al*., Intrinsic magnetic topological insulators in van der Waals layered $MnBi_2Te_4$-family materials. arXiv:1808.08608 [cond-mat.mtrl-sci] (26 August 2018).
111. J. A. Hagmann *et al*., Molecular beam epitaxy growth and structure of self-assembled Bi_2Se_3/Bi_2MnSe_4 multilayer heterostructures. *New J. Phys.* **19**, 085002 (2017). doi: 10.1088/1367-2630/aa759c
112. T. Hirahara *et al*., Large-gap magnetic topological heterostructure formed by subsurface incorporation of a ferromagnetic layer. *Nano Lett.* **17**, 3493–3500 (2017). doi: 10.1021/acs.nanolett.7b00560; pmid: 28545300
113. F. Katmis *et al*., A high-temperature ferromagnetic topological insulating phase by proximity coupling. *Nature* **533**, 513–516 (2016). doi: 10.1038/nature17635; pmid: 27225124
114. D. Jena, A. Konar, Enhancement of carrier mobility in semiconductor nanostructures by dielectric engineering. *Phys. Rev. Lett.* **98**, 136805 (2007). doi: 10.1103/PhysRevLett.98.136805; pmid: 17501230
115. M. M. Ugeda *et al*., Giant bandgap renormalization and excitonic effects in a monolayer transition metal dichalcogenide semiconductor. *Nat. Mater.* **13**, 1091–1095 (2014). doi: 10.1038/nmat4061; pmid: 25173579
116. A. Avsar *et al*., Spin-orbit proximity effect in graphene. *Nat. Commun.* **5**, 4875 (2014). doi: 10.1038/ncomms5875; pmid: 25255743
117. T. Miyazaki, N. Tezuka, Giant magnetic tunneling effect in Fe/Al_2O_3/Fe junction. *J. Magn. Magn. Mater.* **139**, L231–L234 (1995). doi: 10.1016/0304-8853(95)90001-2
118. J. S. Moodera, L. R. Kinder, T. M. Wong, R. Meservey, Large magnetoresistance at room temperature in ferromagnetic thin film tunnel junctions. *Phys. Rev. Lett.* **74**, 3273–3276 (1995). doi: 10.1103/PhysRevLett.74.3273; pmid: 10058155
119. W. H. Butler, X.-G. Zhang, T. C. Schulthess, J. M. MacLaren, Spin-dependent tunneling conductance of Fe|MgO|Fe sandwiches. *Phys. Rev. B* **63**, 054416 (2001). doi: 10.1103/PhysRevB.63.054416
120. J. Mathon, A. Umerski, Theory of tunneling magnetoresistance of an epitaxial Fe/MgO/Fe(001) junction. *Phys. Rev. B* **63**, 220403(R) (2001). doi: 10.1103/PhysRevB.63.220403
121. S. S. P. Parkin *et al*., Giant tunnelling magnetoresistance at room temperature with MgO (100) tunnel barriers. *Nat. Mater.* **3**, 862–867 (2004). doi: 10.1038/nmat1256; pmid: 15516928
122. S. Yuasa, T. Nagahama, A. Fukushima, Y. Suzuki, K. Ando, Giant room-temperature magnetoresistance in single-crystal Fe/MgO/Fe magnetic tunnel junctions. *Nat. Mater.* **3**, 868–871 (2004). doi: 10.1038/nmat1257; pmid: 15516927
123. G.-X. Miao, M. Müller, J. S. Moodera, Magnetoresistance in double spin filter tunnel junctions with nonmagnetic electrodes and its unconventional bias dependence. *Phys. Rev. Lett.* **102**, 076601 (2009). doi: 10.1103/PhysRevLett.102.076601; pmid: 19257701
124. M. Arai *et al*., Construction of van der Waals magnetic tunnel junction using ferromagnetic layered dichalcogenide. *Appl. Phys. Lett.* **107**, 103107 (2015). doi: 10.1063/1.4930311
125. T. Song *et al*., Giant tunneling magnetoresistance in spin-filter van der Waals heterostructures. *Science* **360**, 1214–1218 (2018). doi: 10.1126/science.aar4851; pmid: 29724908
126. D. R. Klein *et al*., Probing magnetism in 2D van der Waals crystalline insulators via electron tunneling. *Science* **360**, 1218–1222 (2018). doi: 10.1126/science.aar3617; pmid: 29724904
127. H. H. Kim *et al*., One million percent tunnel magnetoresistance in a magnetic van der Waals heterostructure. *Nano Lett.* **18**, 4885–4890 (2018). doi: 10.1021/acs.nanolett.8b01552; pmid: 30001134
128. Z. Wang *et al*., Tunneling spin valves based on Fe_3GeTe_2/hBN/Fe_3GeTe_2 van der Waals heterostructures. *Nano Lett.* **18**, 4303–4308 (2018). doi: 10.1021/acs.nanolett.8b01278; pmid: 29870263
129. D. Ghazaryan *et al*., Magnon-assisted tunneling in van der Waals heterostructures based on $CrBr_3$. *Nat. Electron.* **1**, 344–349 (2018). doi: 10.1038/s41928-018-0087-z
130. J. B. S. Mendes *et al*., Spin-current to charge-current conversion and magnetoresistance in a hybrid structure of graphene and yttrium iron garnet. *Phys. Rev. Lett.* **115**, 226601 (2015). doi: 10.1103/PhysRevLett.115.226601; pmid: 26650313
131. S. Dushenko *et al*., Gate-tunable spin-charge conversion and the role of spin-orbit interaction in graphene. *Phys. Rev. Lett.* **116**, 166102 (2016). doi: 10.1103/PhysRevLett.116.166102; pmid: 27152812
132. C. Cheng *et al*., Spin to charge conversion in MoS_2 monolayer with spin pumping. arXiv:1510.03451 [cond-mat.mes-hall] (6 June 2016).
133. J. B. S. Mendes *et al*., Efficient spin to charge current conversion in the 2D semiconductor MoS_2 by spin pumping from yttrium iron garnet. *Appl. Phys. Lett.* **112**, 242407 (2018). doi: 10.1063/1.5030643
134. W. Zhang *et al*., Research update: Spin transfer torques in permalloy on monolayer MoS_2. *APL Mater.* **4**, 032302 (2016). doi: 10.1063/1.4943076
135. D. MacNeill *et al*., Control of spin-orbit torques through crystal symmetry in WTe_2/ferromagnet bilayers. *Nat. Phys.* **13**, 300–305 (2017). doi: 10.1038/nphys3933
136. Q. Shao *et al*., Strong Rashba-Edelstein Effect-induced spin-orbit torques in monolayer transition metal dichalcogenide/ferromagnet bilayers. *Nano Lett.* **16**, 7514–7520 (2016). doi: 10.1021/acs.nanolett.6b03300; pmid: 27960524
137. Q. Sun, N. Kioussis, Prediction of manganese trihalides as two-dimensional Dirac half-metals. *Phys. Rev. B* **97**, 094408 (2018). doi: 10.1103/PhysRevB.97.094408
138. M. Ashton *et al*., Two-dimensional intrinsic half-metals with large spin gaps. *Nano Lett.* **17**, 5251–5257 (2017). doi: 10.1021/acs.nanolett.7b01367; pmid: 28745061
139. J. He, S. Li, Two-dimensional Janus transition-metal dichalcogenides with intrinsic ferromagnetism and half-metallicity. *Comput. Mater. Sci.* **152**, 151–157 (2018). doi: 10.1016/j.commatsci.2018.05.049
140. S.-J. Gong *et al*., Electrically induced 2D half-metallic antiferromagnets and spin field effect transistors. *Proc. Natl. Acad. Sci. U.S.A.* **115**, 8511–8516 (2018). doi: 10.1073/pnas.1715465115; pmid: 30076226
141. R. Brec, Review on structural and chemical properties of transition metal phosphorous trisulfides MPS_3. *Solid State Ion.* **22**, 3–30 (1986). doi: 10.1016/0167-2738(86)90055-X
142. M. A. McGuire, Crystal and magnetic structures in layered, transition metal dihalides and trihalides. *Crystals* **7**, 121 (2017). doi: 10.3390/cryst7050121
143. M. A. Susner, M. Chyasnavichyus, M. A. McGuire, P. Ganesh, P. Maksymovych, Metal thio- and selenophosphates as multifunctional van der Waals layered materials. *Adv. Mater.* **29**, 1602852 (2017). doi: 10.1002/adma.201602852; pmid: 28833546

144. A. Banerjee *et al*., Neutron scattering in the proximate quantum spin liquid α-$RuCl_3$. *Science* **356**, 1055–1059 (2017). doi: 10.1126/science.aah6015; pmid: 28596361
145. K. Xu *et al*., Ultrathin nanosheets of vanadium diselenide: A metallic two-dimensional material with ferromagnetic charge-density-wave behavior. *Angew. Chem. Int. Ed.* **52**, 10477–10481 (2013). doi: 10.1002/anie.201304337; pmid: 23956052
146. Y. Zhou, H. Lu, X. Zu, F. Gao, Evidencing the existence of exciting half-metallicity in two-dimensional $TiCl_3$ and VCl_3 sheets. *Sci. Rep.* **6**, 19407 (2016). doi: 10.1038/srep19407; pmid: 26776358
147. X. Bourdon, V. Maisonneuve, V. B. Cajipe, C. Payen, J. E. Fischer, Copper sublattice ordering in layered $CuMP_2Se_6$ (M = In, Cr). *J. Alloys Compd.* **283**, 122–127 (1999). doi: 10.1016/S0925-8388(98)00899-8
148. M. A. McGuire, F. J. DiSalvo, $Ni_3Cr_2P_2Q_9$ (Q = S, Se): New quaternary transition metal chalcogenides with a unique layered structure. *Chem. Mater.* **19**, 4600–4605 (2007). doi: 10.1021/cm070849f
149. S. Liu *et al*., Wafer-scale two-dimensional ferromagnetic Fe_3GeTe_2 thin films grown by molecular beam epitaxy. *NPJ 2D Mater. Appl.* **1**, 30 (2017). doi: 10.1038/s41699-017-0033-3
150. D. Sander *et al*., The 2017 magnetism roadmap. *J. Phys. D Appl. Phys.* **50**, 363001 (2017). doi: 10.1088/1361-6463/aa81a1

ACKNOWLEDGMENTS

Funding: Supported by NSF grant EFMA-1542741 and King Abdullah University of Science and Technology (KAUST) Office of Sponsored Research award OSR-2016-CRG5-2996. **Competing interests:** None declared.

10.1126/science.aav4450

Science

Two-dimensional magnetic crystals and emergent heterostructure devices

Cheng Gong and Xiang Zhang

Science **363** (6428), eaav4450.
DOI: 10.1126/science.aav4450

The ultimate in thin-film magnetism

The alignment of the magnetic properties of atoms gives rise to a wealth of simple and exotic properties that can be exploited. As the dimension of the material is reduced, such that the atoms are in a single monolayer, it was widely believed that thermal fluctuations overwhelm and prevent magnetic ordering. Gong and Zhang review the developments that have followed the recent discovery of magnetism in two-dimensional materials. Recognizing that magnetic anisotropy can be used to induce stable magnetism in atomic monolayers, they provide an overview of the materials available and the physical understanding of the effects and then discuss how these effects could be exploited for widespread practical applications.

Science, this issue p. eaav4450